Channel Guided Standard LWFA (CGSL) Project

Final Report
Icarus Research Inc.
December 2005

Executive Summary

The Phase II Icarus CGSL project was initiated at July 1 2003. This report is summarizing the project activities and achievements of this project

I. The modified work plan includes the following tasks.

1. *Capillary Plasma Channel Generation*
- Fabricate and test 10^{18} cm^{-3} ablative-wall capillary
- Technical issues 5 axis (x-y-z☐)control , laser trigger
- Characterize plasma density and profile; (interferometer)
- Guiding experiments with T^3 laser at low power

2. *Multi-stage Channel Guiding*
- Fabricate and test segmented capillaries
- Characterize plasma of individual stages
- Demonstrate multi-stage guiding using T^3; comparison with TurboWAVE PIC simulations

3. *Guiding in Standard LWFA Regime*
- Incorporate TFL (Terawatt Femtosecond Laser) into target chamber beamline
- Install optics for matched injection into channel ($r_0 \sim r_M \sim 30$ μm)
- Demonstrate guiding at 1 TW, $r_0 \sim r_M$, $c\tau_L \sim 0.5\lambda_p$

4 *High Power Guiding and Acceleration*
- Test pump laser for 10 TW system
- Set up 10 TW LWFA experimental beamline
- Optical injection of MeV electrons into channel; optimization with TurboWAVE PIC simulations and CyberRay™.
- Optimize injection timing using intercepting diagnostic for accelerated electrons (film, Čherenkov, magnetic spectrometer)
- Demonstrate single stage standard LWFA guiding at high power (>5 TW, 10^{18} cm^{-3}, matched injection); optimize with TurboWAVE PIC simulations
- Measure spectrum of accelerated electrons from single-stage LWFA using magnetic spectrometer

The major tasks of the project were accomplished with significant success. During the project we have demonstrated control of several important parameters of capillary channels. We achieved the required profiles for guiding, we have demonstrated channels in density range between 10^{17}-10^{19}cm^{-3} in both short and long capillaries. The plasma temperature and density profiles were measured in both radial and longitudinal directions. The Boron Nitride capillary has provided a guiding medium that can withstand more than 1000 shots. The laser ignition of capillary discharge provided reliable almost jitter free approach. Both laser and experimental set up were upgraded. The laser system upgrade included development of a 10 TW Ti-sapphire laser facility that will be used for acceleration experiments instead T cube. We have conducted high intensity (above 10^{17}W/cm^2) guiding experiments through various capillaries. The concerns related to influence of relatively high current density flow through capillary on the injected electrons were studied extensively by us both theoretically and experimentally using a simple injection method. The method is based on the interaction of a high intensity laser pulse with a thin wire placed near capillary entrance. The influence of magnetic fields was found to be insignificant. Using this method we have studied transport of electrons though capillary discharge. We have simulated beam injection into a channel guided LWFA and found that under certain conditions the injected electron distribution can be very broad. Finally, prior to the staging of the capillary based accelerators, we performed a proof-of-principal experiment on staged optical injection and laser wakefield acceleration using two different short laser pulses focused into two spatially separated gas jets. The report includes the following sections:

1. Fabricate and test 10^{18} cm^{-3} ablative-wall capillary
2. Characterize plasma density and radial profile
3. Capillary discharge experimental results:
    A. Boron nitride capillary discharge
    B. Low – current polyethylene capillary discharge

4. Longitudinal profiles of plasma parameters in a laser-ignited capillary discharge and implications for laser wakefield accelerator applications

5. Laser and experimental set up upgrade

    A. Laser system upgrade.
    B. Experimental system up-grade

6. Guiding experiments

7. Electron Propagation through capillary

a. Measurements of electron energy spectra

   b. Interpretation of electron energy spectra

   c. Transport of electrons through a capillary discharge

   d. Simulation of beam injection into a channel-guided lwfa

8. Staged all-optical laser wakefield acceleration.

Report of Phase II Research

1. <u>Fabricate and test 10^{18} cm^{-3} ablative-wall capillary</u>

Using laser trigger we have modified the capillary circuit –we have eliminated the need for electrical trigger- we have reduced the delay and jitter of the channel. There are initial indications that the achieved plasma profile is deeper (Depth of the channel), this feature will be of high importance for very high guided laser intensities .Moreover, we have eliminated the electrical interferences. The required plasma density conditions were found and achieved.

2. <u>Characterize plasma density and radial profile</u>*:*

   The density and radial profile of the plasma channel were measured using spectroscopic and (not interferometric) techniques to analyze the plasma at the end of the capillary. Using 20 nf capacitor , 35 ohm resistor and 10KV we were able to obtain 2-3 10^{18} cm^{-3} electron densities. The measurements were done using spectral lines emitted by Hydrogen and Carbon. The design was supported by 1-D MHD simulations of the capillary plasma. The density profile was measured (see below), and the optimal condition for guiding were found by guiding laser beam through capillary during various delay times and measuring the energy transmission. We have been able to transfer 75% through 3cm capillary.

3. Capillary discharge <u>experimental results:</u>

  A.Boron nitride capillary discharge

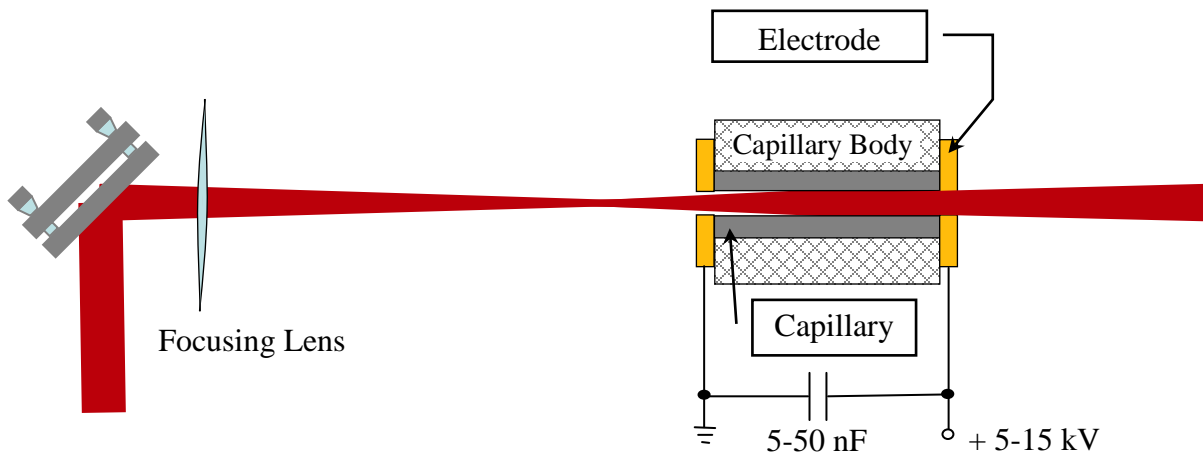 B.   Low – current polyethylene capillary discharge

A. BN capillary discharge

Fig.3.1. Experimental setup BN capillaries, d = 0.3 – 0.4 mm, l = 10 – 15 mm; C = 50 nF, U = 4 – 20 kV, L $\approx$ 1 μH ; (I_m = 500 – 2500 A, i_m = 4x10^6 – 3x10^7 A/cm^2)., Laser ignition: 10-20mj, 10 ns, 1.064 μm.
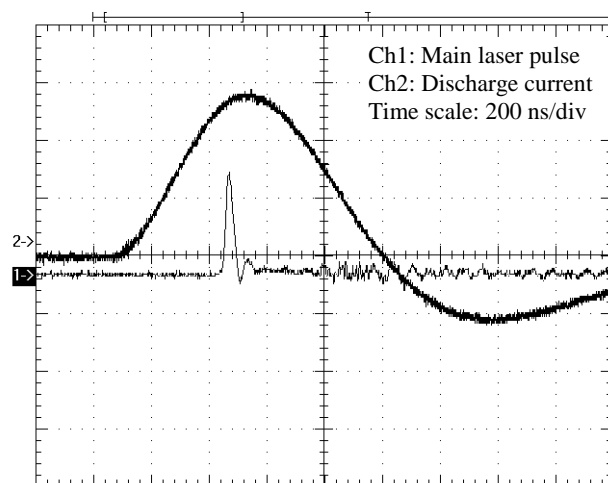

Fig. 3.2. Temporal profile of the capillary discharge current (10 kV)

Horizontal scale: 200 ns per large division Vertical scale: 500 A per division, BN capillary: d = 0.3 mm, l = 15 mm.

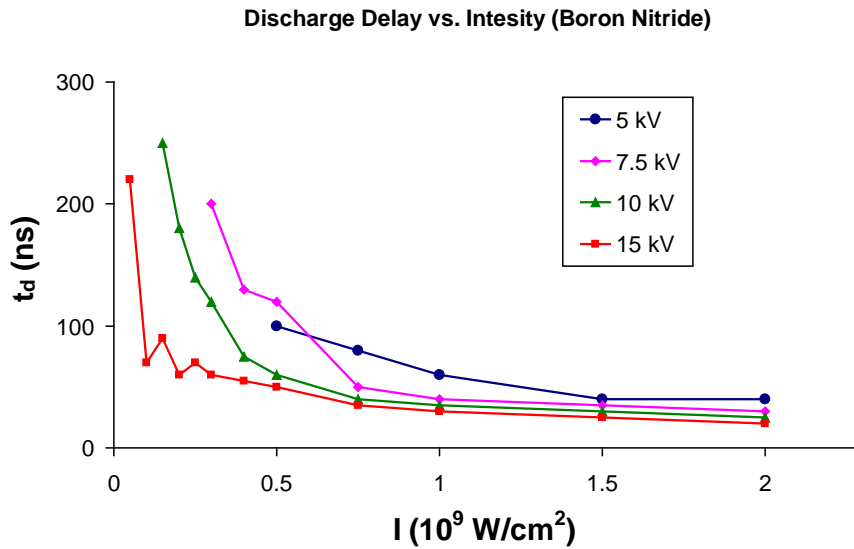**Discharge Delay vs. Intesity (Boron Nitride)**

Fig. 3.3. Boron nitride capillary (10 mm long, 0.3 mm diameter). Delay of discharge breakdown vs incident laser intensity at different voltages.
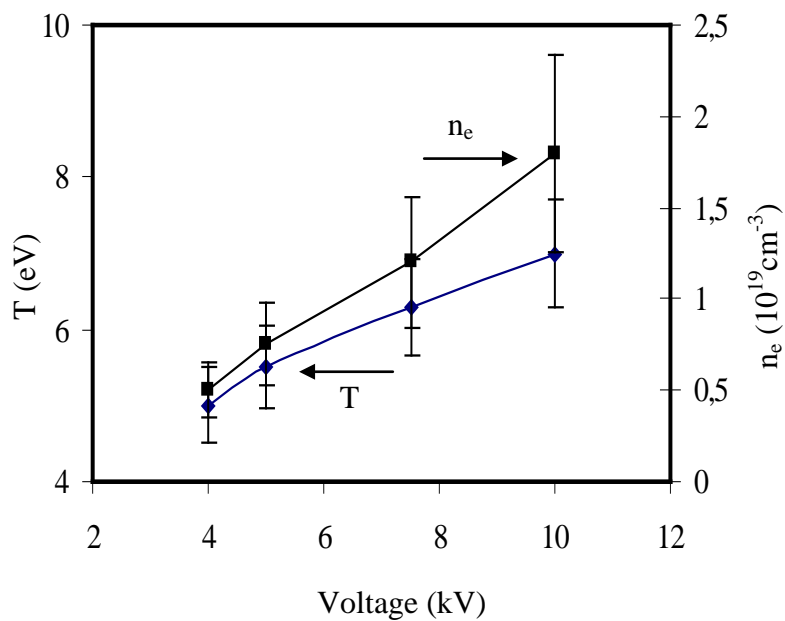

Fig. 3.4 Plasma temperature and electron density at the axis of capillary vs discharge voltage at 400 ns delay from the beginning of discharge. BN capillaries, d= 0.3 mm, l = 15 mm. U = 12 -18 kV, T ≥ 8 – 10 eV (Observation of NV lines in XUV region)

6
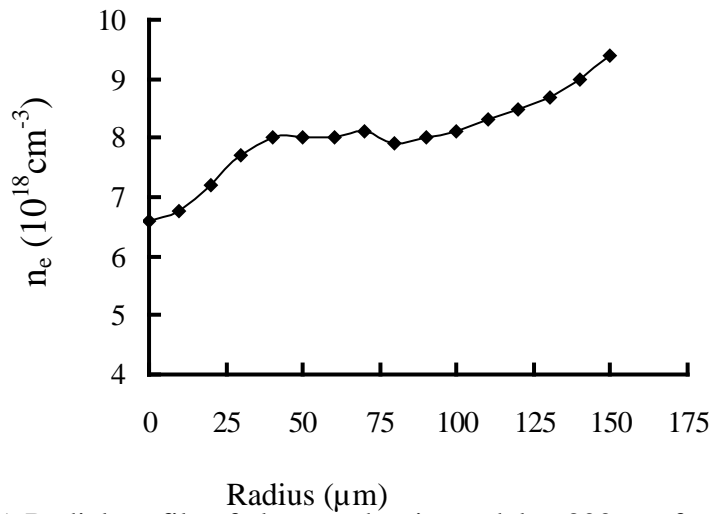
Fig 3.5. Radial profile of electron density at delay 300 ns after the discharge start BN capillary, (10 kV), d = 0.35 mm, l = 15 mm, ICCD gate period- 20 ns.

Transient electron density hole at the axis after beginning of the explosive secondary ablation

Electron density profiles for different moments:
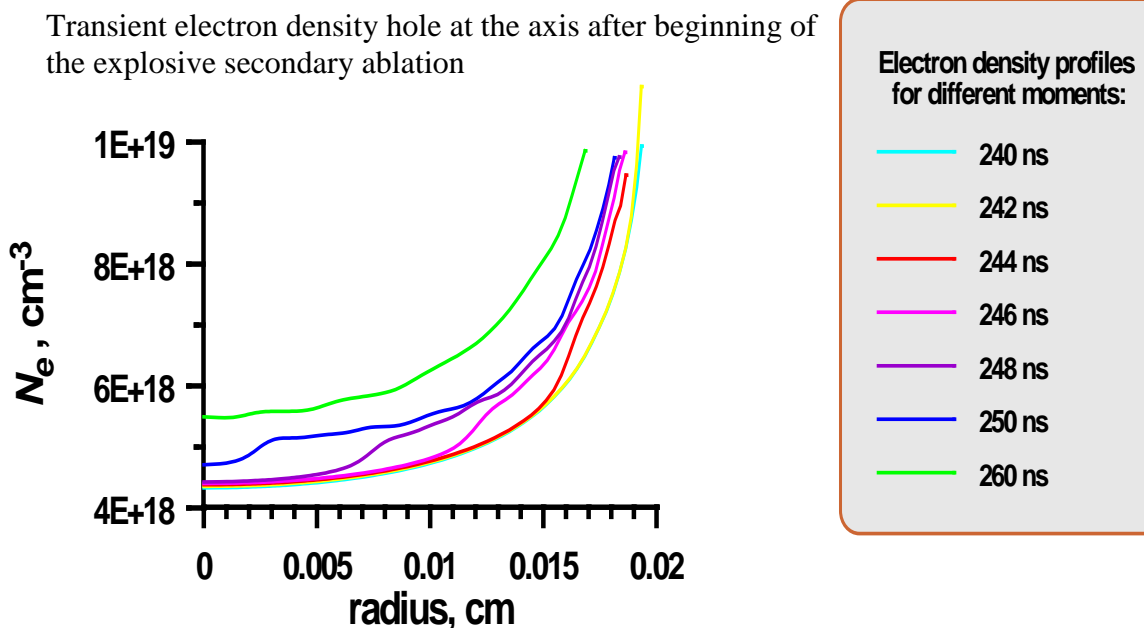
240 ns
242 ns
244 ns
246 ns
248 ns
250 ns
260 ns

Fig. 3,6 Simulation of capill. diam = 0.4 mm; density hole diam = 0.3 mm; density = 0.1 mg/cm^3; $N_0 = 4.3 \cdot 10^{18}$ cm^{-3}; $v_0 = -1$ km/s; the EOS is so that the ablation starts at ~5100 °C and 104 bar

Comments

- For the BN capillary, the second ablation starts at about 200-300 ns.

- The capillary is filled quickly by dense plasma after beginning of the secondary ablation.

- The front of the filling wave is sharp.

- The effect may cause formation of a transient electron density hole at the axis. It takes place just before the moment when the filling wave reaches the axis.

B. Low – current $(CH_2)_n$ ablative capillary discharge

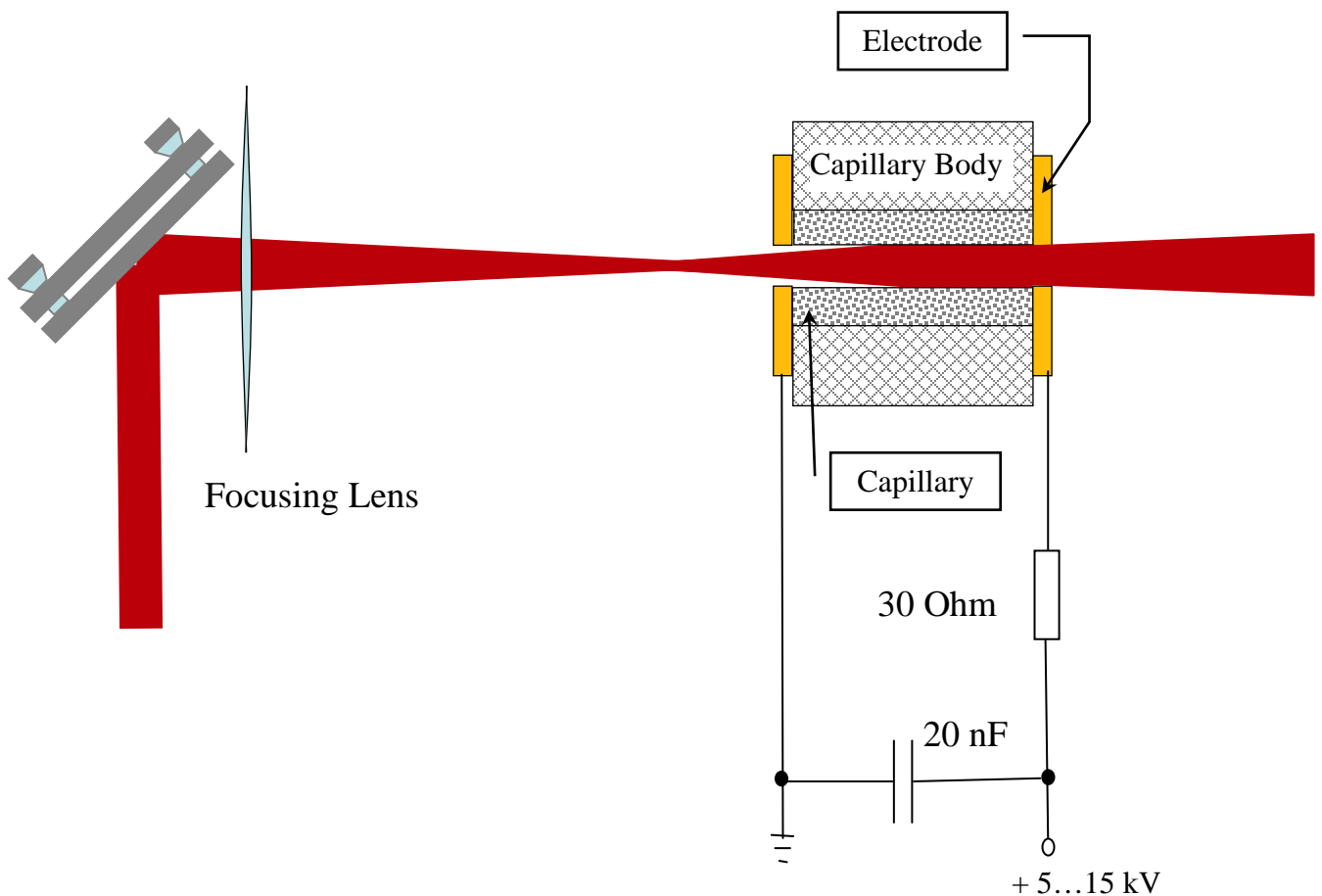Fig. 3.7. Experimental setup Polyethylene capillaries, d= 0.5 mm, l = 15 mm; C = 20 nF, U = 5 – 10 kV, R ≈ 30 Ω; (I_m = 150 – 300 A, i_m = (0.75 – 1.5) x 10^5 A/cm^2). Laser ignition: $(1 – 4) \times 10^8$ W/cm^2, 10 ns, 1.064 μm.

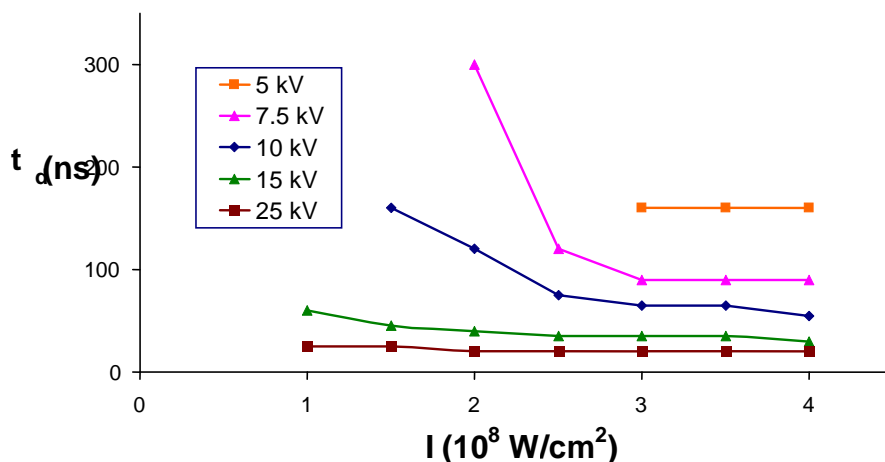**Discharge Delay vs. Intensity (Polyethylene)**

Fig. 3.8 Breakdown delay for a polyethylene capillary (15 mm long, 0.5 mm diameter) vs incident laser intensity at different voltages.
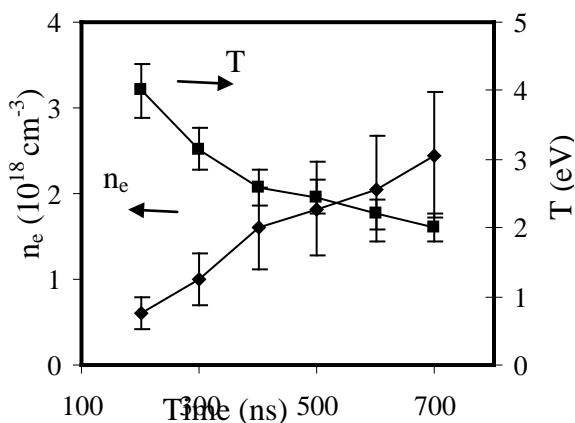Measured electron density and temperature:

Fig. 3.9 Electron temperature and density
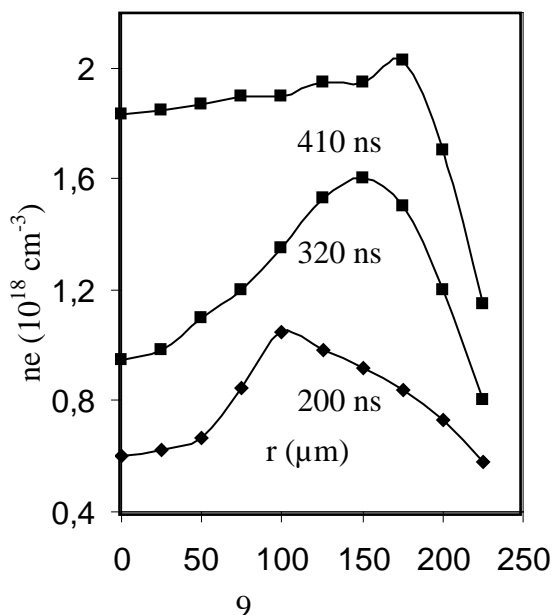at the axis of the capillary discharge (7.5 kV) as function of time.

Fig. 3.10. Radial profiles of electron density at different delays from the beginning of discharge ($I_m = 200A$).

4. Longitudinal profiles of plasma parameters in a laser-ignited capillary discharge and implications for laser wakefield accelerator applications

A laser pulse entering the capillary during the discharge can be guided when the plasma refraction index peaks on the capillary axis. To obtain a proper guiding condition, the electron plasma density of the channel and the off-axis density gradient must be matched with the duration and focal size of the guided laser pulse, respectively. The radial density profile was the subject of a number of earlier works. The knowledge of longitudinal distribution of plasma parameters in capillary discharges is important for the proper coupling of laser beam to the plasma, phase matching of injected electrons into the channel, and staging of several channels. In particular, plasma channels with longitudinally varying electron density have been proposed to increase the dephasing length and, consequently, the energy gain of laser wakefield accelerators. This technique is based on piecewise formation of the longitudinal profile, and assumes uniform longitudinal electron density along each capillary piece of constant diameter. Interferometric measurements of the axial variation of plasma density have been made in a transparent square plasma capillary discharge,[1] but this configuration is not well-suited for most guiding applications.

Here we report on the measurements of longitudinal electron density and temperature profiles in plasma produced in a cylindrical, low-current Plexiglas capillary discharge with laser ignition. Plasma radiation was observed through a lateral wall of the capillary. Plexiglas has a good transmission in the UV range from 315 to 380 nm (≥ 70 %) and in the visible range from 380 to 780 nm (≥ 90 %).[2] The experimental setup is shown schematically in Fig. 4.1.

The Plexiglas capillary had a diameter of 0.5 mm and a length of 15 mm. The discharge occurred in a vacuum chamber evacuated below 10^{-4} Torr. To ignite the discharge, we used a 1.064 µm, 10 ns pulse from an Nd-YAG laser. This laser ignition technique[15] ablates a small amount of material from the inner wall of the capillary and produces seed ionization that triggers the discharge after ~50 ns. The energy required for reliable ignition was 10 to 15 mJ. This technique makes it possible to achieve very low (less than 10 ns) shot-to-shot jitter of the ignition delay.[15]

The parameters of the discharge circuit and the driving voltage were typically chosen to provide a peak current of 200 A and relaxation time of 600 ns. The current rise time was measured to be about 100 ns. Current waveforms of 300 consecutive shots exhibited very little shot-to-shot variations. They were obtained using a Rogowsky coil and a 300 MHz Tektronix oscilloscope.

The information about the dynamics of plasma column was derived from streak photographs obtained at a rate of 20 ns/mm collected by an IMACON-700 camera. The images indicated that the electric breakdown began on the capillary axis, and the plasma column maintained axial symmetry during the discharge.

The spectra emitted by the discharge plasma were investigated in the range 300 – 800 nm using SpectraPro 275 Acton spectrograph equipped with 2400 grooves/mm grating and Princeton Instruments Intensified Photodiode Array (IPDA) detector. The system included a turning mirror which allowed for scanning along the capillary axis. With 30 µm entrance slit, the spectral resolution of the optical system was about 0.1 nm. The gate-on time of the IPDA detector was 50 ns.

We obtained longitudinal profiles of the continuum and the spectral lines at different delays with respect to the beginning of the discharge. Lines of carbon atoms C I, carbon ions C II, C III, oxygen ion O II and hydrogen H_α line were observed.
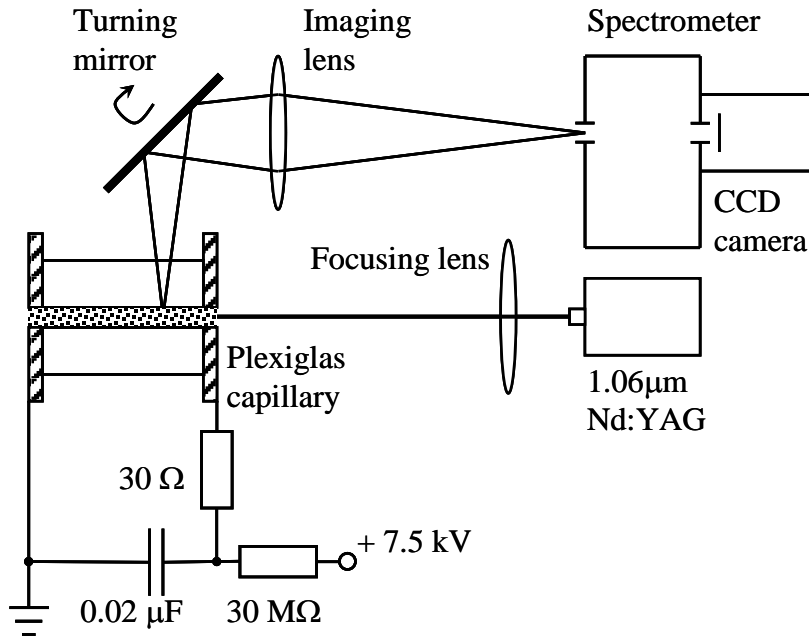
.Fig 4.1 Experimental setup.

(a)
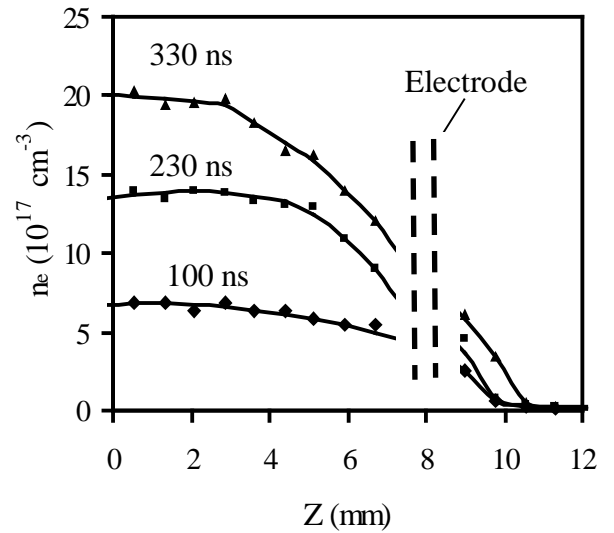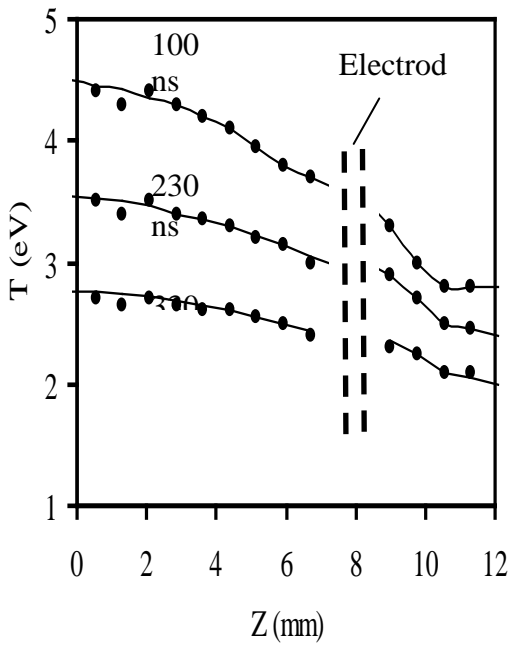
(b)

Fig. 4.2. Longitudinal profiles of (a) plasma temperature and (b) electron density at three different delay times from the triggering of the discharge.

Plasma temperature was estimated from the relative intensities of singly-ionized carbon emission lines C II 462.7 nm and C II 387.6 nm, and was found to be between

2 and 4.5 eV. Fig. 2a shows longitudinal temperature distributions at three different times after the beginning of the discharge. It is seen that the temperature at the capillary end drops by 15 – 20 % with respect to that in the middle. In the near-outlet region of the plasma jet, the temperature undergoes a further drop of the same order of magnitude.

Electron density was determined from the broadening of the H_α line.[4,5] Under our experimental conditions, Stark effect is the dominant line broadening mechanism, and the broadening parameters are weak functions of plasma temperature.[4] Fig. 4. 2b shows axial distribution of electron density (averaged over the plasma column diameter) at three different times. It is seen that, as the discharge develops, the relative reduction of electron density near capillary ends increases. At 100 ns from the beginning of the discharge the electron density at the capillary opening falls by a factor of 1.3 as compared to that in the middle. At 330 ns, this factor is about 1.7. The electron density decreases sharply in the near-outlet region of the plasma jet. In fact, at a distance of four capillary diameters the electron density falls to a few percent of its initial value.

The variation in plasma density does not appear to interfere significantly with the coupling of the laser pulse into the channel. This is probably due to the fact that the plasma is multiply ionized even in the transition region outside, so ionization defocusing effects[6] are probably small. However, this density variation may present substantial difficulties for externally-injected electrons in a channel-guided standard laser wakefield accelerator (CGS-LWFA). In the CGS-LWFA concept, laser and plasma channel parameters are chosen so that the laser propagates at nearly constant spot size and produces a large amplitude plasma wave or wakefield that can trap and accelerate injected electrons. The wakefield phase velocity is near the group velocity v_g of the driving laser pulse, and its wavelength is near the on-axis plasma wavelength λ_p, where $\lambda_p = (\pi c^2 m_e/e^2 n_{e0})^{1/2}$, c is the velocity of light, e and m_e are the electron charge and mass, and n_{e0} is the on-axis plasma electron density.

Electrons injected into the wakefield with initial velocity $v_0 < v_g$ can be accelerated to high energy provided they remain in portions of the wakefield that have an accelerating longitudinal electric field and a confining or focusing radial electric field. In a uniform plasma, this accelerating and focusing region corresponds to exactly one-quarter of the wave period. In a plasma channel with no axial variation in

density, recent analytical and simulation studies have shown[7,8] that the channel introduces a favorable shift in the wakefield phases that are both focusing and accelerating, thereby reducing the minimum injection energy for trapping and increasing allowable acceleration (dephasing) length and final energy.

However, if electrons are injected externally, they must traverse a region where the density n_{e0} increases continuously with z, and $\lambda_p(z) \sim (n_{e0}(z))^{-1/2}$ decreases. This continuous change in the plasma wavelength implies that particles that are injected into accelerating buckets that are far behind the laser pulse will always experience a defocusing electric field and are likely to be lost. Particles that are introduced into the wake immediately behind the laser pulse are less affected by this defocusing problem but must cross a transition region where the wakefield accelerating field is relatively weak and are likely to fall too far behind the laser pulse.

These effects are readily apparent in turboWAVE simulations of a CGS-LWFA that uses the 100 ns delay axial plasma density profile shown in Fig. 2. The laser had a peak power $P_0 = 8$ TW, wavelength $\lambda_0 = 0.8$ μm, and vacuum focal spot size $r_0 = 30$ μm. The radial profile of the plasma was chosen so that the equilibrium or matched radius was equal to r_0. The laser and plasma parameters are similar to those used in the earlier simulation studies that assumed a longitudinally uniform plasma channel density.[8] Separate bunches of test particle electrons were injected over a range of initial phases with initial energies W_0.

The behavior was substantially different from the simulations reported previously.[19,20] In those simulations, the minimum injection energy for trapping W_- was 1.0 MeV, which was significantly below the theoretical uniform plasma value of 1.6 MeV. However, the presence of the experimentally found long density ramp caused W_- to increase to approximately 4 MeV. In addition, only injected electrons in the first accelerating bucket were trapped, while those in later buckets experienced a defocusing electric field at some point and were ejected from the channel.

Although this appears to be a fundamental problem for injection into a CGS-LWFA, there are several possible solutions. First, the electrons can simply be injected at higher energy, which primarily involves using higher power lasers for optical injection. The second approach is to reduce the density gradient length so that it is short compared with the betatron wavelength of the injected particles, which may be possible by shaping the capillary nozzle or using short segmented capillary

discharges. Reducing the density gradient length by a factor of 5 in the simulation caused W_- to drop to approximately 2 MeV. A third alternative is to perturb the wakefield inside the capillary so that injection is internal.

In conclusion, the evolution of longitudinal electron density and temperature profiles in plasma produced in a low-current Plexiglas capillary discharge with laser ignition was investigated, including the plasma jet transition region near the exit of the capillary. At times when the radial profile of the plasma density is suitable for guiding, the plasma density near the capillary ends can be up to 30 % lower than its value in the center of the capillary. This axial variation in plasma density does not significantly affect the coupling of the laser beam into the capillary. However, simulations show that the density gradient may make external injection of electrons into a laser wakefield accelerator significantly more difficult.

5. Laser and experimental set up upgrade

A. Laser system upgrade.

All previous experiments were done on T-Cubed laser system. The main disadvantages of the system are complicity, low stability, and low repetition rate. The T-Cubed laser requires many hours of daily alignment procedure and special control for pointing and energy stability. The main amplifier of the system takes 15 to 20 minutes to cool down and to be ready for the next shot. During this time some critical parameters of the system could being change and an attempt of repeating the previous result would fail. In order to collect enough valid and reliable data we had to perform very long continuous runs of 20 hours and more. The energy stability of this class laser system is usually worth then 15%. After double passing the 9 mm amplification stage we improved this parameter down to 10%. But it still can not compete with modern TiS lasr systems.

The main experimental task this year was to switch the LWFA experiment from the old, single shot T-Cubed system, to a new 10 Hz, 50 femtosecond laser (TFL). The new laser allowed not only to collect more data in a shorter time, but also to work in the standard LWFA regime. Using this regime, external injection of electrons, and guiding of acceleration laser beam could make possible creation of compact high energy accelerators. But for the standard LWFA the plasma density in the guiding structure must match the laser pulse length. For 500 fs laser pulse the plasma density should be about 5×10^{16} cm^{-3}. It is very difficult to create stable, no

leaky channel of such low density. For 50 fs pulse, however, the plasma density should be 5×10^{18} cm^{-3}. Optical guiding at these conditions was demonstrated by many experimental groups. The main amplifier of the TFL laser was recently upgrade from 4-pass to 5-pass, that allowed to get 800 mJ before compression of the beam. This beam is spitted into 700 mJ and 100 mJ portions using CVI low dispersion polarizer and zero-order waveplate. The 700 mJ beam goes through a beam expander into vacuum compressor. The 50 fs, 10 TW beam is sent to the main experimental chamber. This beam is going to be used for acceleration in the capillary plasma channel. The 100 mJ beam first is going through an adjustable delay line into an air compressor. Compressed 1.5 TW beam is sent to the main experimental chamber. This beam will be used to inject electrons from the gas jet.

In our recent setup we consider to use two different approaches for electron injection. The first one is the same SM-LWFA injection, used the in previous experiment. The advantage of this scheme is large number of injected electrons for relatively low intensity (1-2 TW) injection laser beam. The disadvantage is, as we discovered in the previous experiment, the tight alignment between injection and acceleration laser beams. A 10 μm misalignment between the focal spots decreased the number of high energy electrons to undetectably low level. This high sensitivity is a result of ponderomotive expulsion of misaligned electrons by the acceleration laser beam. As the injected electrons propagate from the first to the second jet, they are overtaken by the acceleration laser pulse, and are exposed to a large radial ponderomotive force. The pondermotive potential of the nearly focused beam is strong enough to deflect the low energy injection electrons and therefore to direct these electrons away from the accelerating structure. Only particles very close the laser axis, where the ponderomotive force vanishes, can be trapped and accelerated.

The other proposed injection scheme is high density laser ionization and ponderomotive acceleration (HD-LIPA). The advantage of this scheme is higher energy electrons and relatively simple alignment. In HD-LIPA the largest number of the injected electrons is offset from the laser propagation direction. As the result this electrons can avoid pondermotive deflection by the acceleration beam. The disadvantages of this scheme are higher injection beam intensity and smaller number of the injection electrons.

New setup of experimental system.

The other ongoing experimental project is to integrate the ablative discharge capillary device into the electron injection-acceleration experiment. The tests of a new laser-triggered capillary were finished last year. This capillary can create long, stable plasma channel. Compare to the double capillary discharge, the laser-triggered capillary create less electrical noise and could be operated in electrically sensitive environment. A new 5 motorized axis mount was designed and build to hold the capillary. Processing compatibility of the gas jet and the capillary was tested. For the initial set of experiments we are going to use 1 cm long capillary. The 5 cm long capillary is also ready for use. In order to keep the standard LWFA regime the plasma density in the capillary should be about 5×10^{18} cm^{-3}. Recent experiments demonstrated optical guiding through the 3 cm long capillary with the plasma density below 10^{17} cm^{-3}.

The electron spectrometer we used in previous experiments is supplemented now by the second stage. The old stage (6.6 cm 0.275 T) will be used to analyze injection and low energy (up to 10 MeV) accelerated electrons. The new stage (15 cm 1.2 T) is able to resolve electrons up to 200 MeV. The new Andor image intensifier camera was installed to image the scintillator. For higher energy electrons a larger magnet is required. In addition to the conventional magnetic electron spectrometer we consider to use fission nuclear activation.

6. Guiding Experiments:

The guiding was obtained using T^3 laser

High resolution guiding image

300 µm diameter capillary. 1 TW laser power. > 70% transmition efficiency.

150 µm
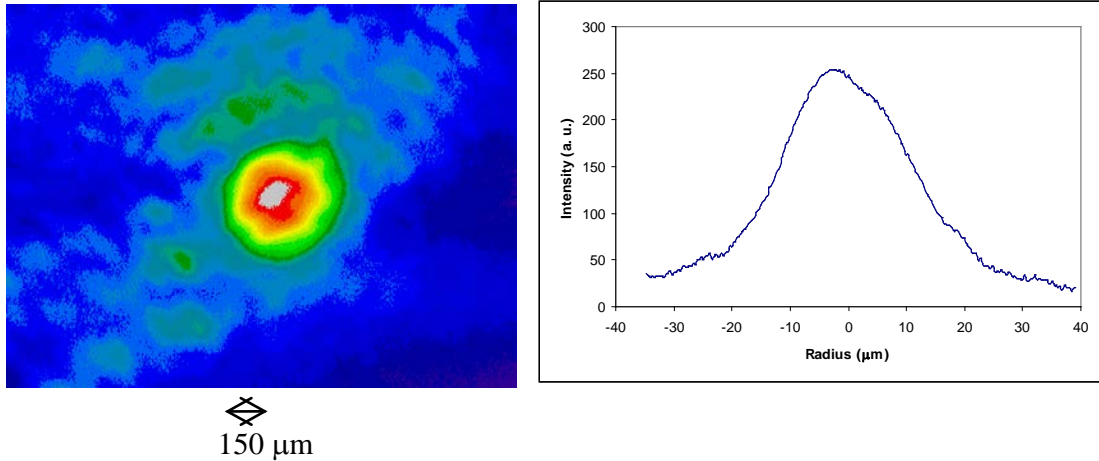
7. Electron Propagation through capillary

One of concerns in development of capillary discharge for guiding and acceleration was the influence of electrical current and corresponding magnetic field on deflecion of injected electrons. For this purpose we designed an experiment based on all optical electron injector using an intense ultrashort pulse laser and a solid wire target and transmitted electrons through capillary.

EXPERIMENTAL SETUP

The experiments were conducted using a TW short pulse Ti-sapphire laser with a wavelength of 800 nm. The laser delivered 45 fs FWHM pulses with a maximum energy up to 600 mJ at a pulse repetition rate of 10 Hz. A schematic drawing of the experimental set up is shown in Figure 7.1.
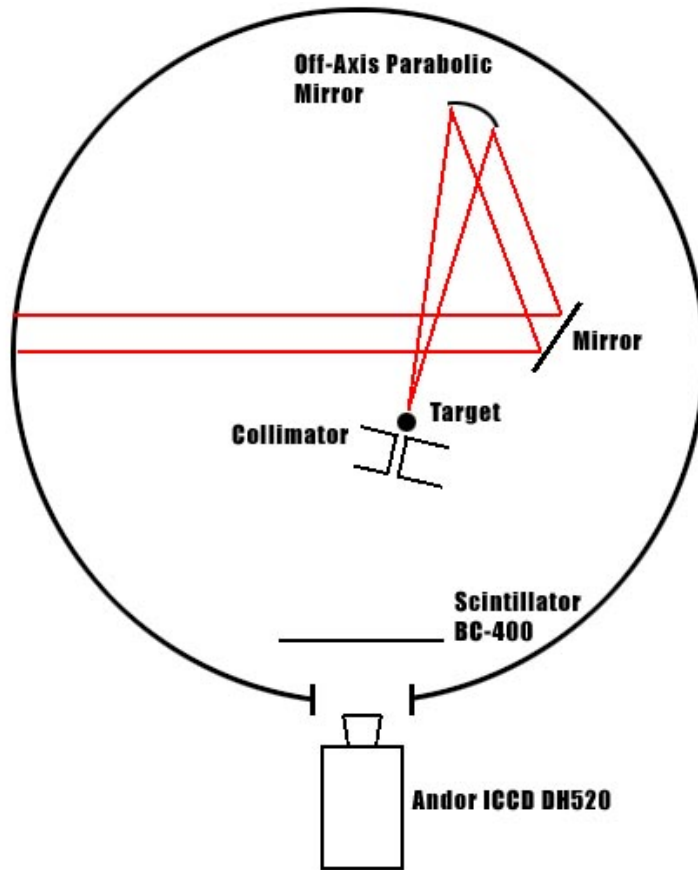
Fig 7.1 Experimental setup. The laser is focused by an off-axis parabola onto a wire target, producing energetic electrons. These electrons pass through a collimator and are deflected by a vertical magnetic field and detected by the scintillator.

The laser beam was focused to a 30 μm diameter spot using an f/6 off-axis parabolic mirror at perpendicular incidence with respect to the target. The maximum intensity in the focal plane was estimated to be about 10^{18} W/cm^2. The contrast ratio of the main pulse to the prepulse that precedes it by 8 ns was greater than 10^4. The targets were solid tungsten wires 13 μm wide. For purpose of comparison, electron generation from solid 25 μm thick foils tungsten was investigated as well.

The electron energy distribution in the forward direction was measured with a magnetic spectrometer. The detector was a BC-400 scintillator located at 19 cm from the backside surface of the target. The scintillator was 14 cm long and 2.5mm thick and was coupled to an ICCD camera. A cylindrical collimator with an entrance opening of 3 mm was placed between the target and the scintillator. The collimator

was made of 50 mm thick graphite and 5 mm lead. The scintillator was covered with two layers of 20 μm Al foil as a light shield that prevented light penetration without affecting electrons with energies above 100 keV. For electrons in the energy range between 100 keV and few MeV, the number of photons created in this scintillator is proportional to the number of electrons, although there is a difference in penetration depth at different energies. This feature allowed us to obtain the number of electrons and to derive their energy distribution.

MEASUREMENTS OF ELECTRON ENERGY SPECTRA

Figure 7.2 shows an example of the electron image recorded by the ICCD camera in an experiment with a vertical wire target and P laser polarization. The three images correspond to spectrometer magnetic fields of (a) 83 Gauss, (b) 40 Gauss, and (c) zero Gauss. The energy of the electrons was derived from calculation of electron trajectories using a map of the measured magnetic field.

Figures 7.3 and 7.4 show the energy spectrum of electrons generated from wire targets for P and S polarization. The number of electrons calculated from the integrated spectrum was about 1.5×10^6 per pulse for wire targets under laser P polarization. The electron yield was about 20% less for S polarization. The electron density spectrum was peaked at about 600-700 keV. A tail of hotter electrons with energies of up to 3 MeV is seen in the spectrum; however their number is close to the noise level of the detection system. The cutoff on the low energy part of the spectrum can be attributed to the strong space charge field created on the surface of the wire. This field allows escape of only the energetic electrons. The peak of the electron distribution can be controlled by the laser intensity and can be tuned for optimal conditions of electron injection. The curves in Figures 7.3 and 7.4 are Boltzmann fits to the experimental data.

Figure 7.5 shows the energy spectrum of electrons generated from 25 μm thick foil targets for P laser polarization. In this case, the electrons generation is not enhanced for laser P polarization, as expected in the case of a normal incident beam.

The angular distribution of energetic electrons was measured by removing the collimator, surrounding with AGFA D-7 film. The angular distribution of forward electrons and the raw film image are shown in Fig. 7.6. The angular distribution of the electrons emitted in the forward direction shows a beam of collimated electrons

moving within ~ 20° of the direction of laser propagation. This narrow bunch is accompanied by a low intensity ring with an angular spread of ~ 50°.
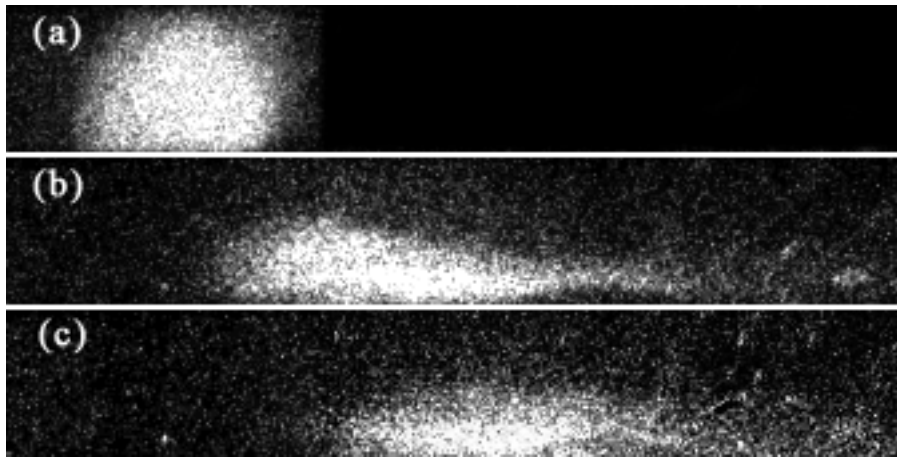

Fig 7.2 The electron image recorded by the ICCD camera in an experiment with a vertical wire target, P laser polarization and a magnetic field of 83 Gauss (a), 40 Gauss (b) and no magnetic field (c).

Fig 7.3 Spectrum of fast electrons measured in the forward laser direction for radiation of a wire target with P laser polarization.
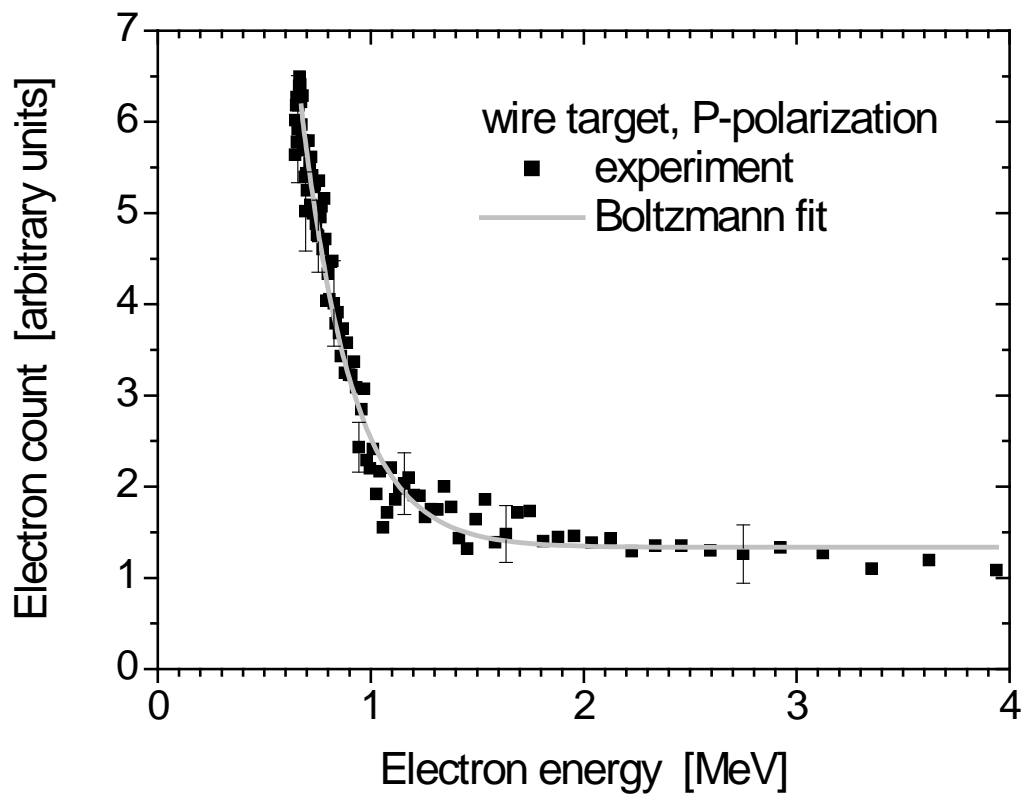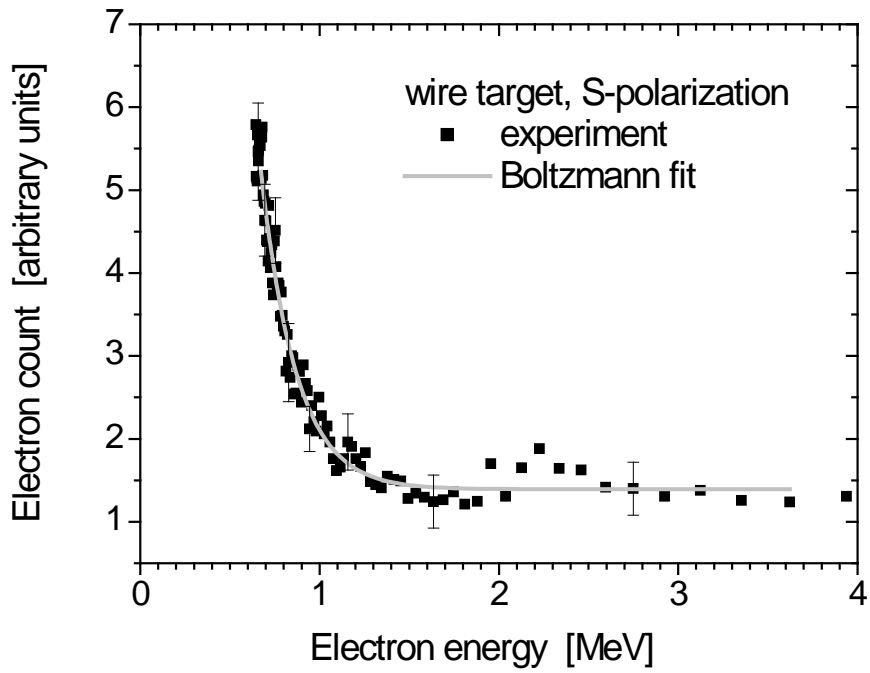
Fig. 7.4 Spectrum of fast electrons measured in the forward laser direction for irradiation of a wire target with S laser polarization.
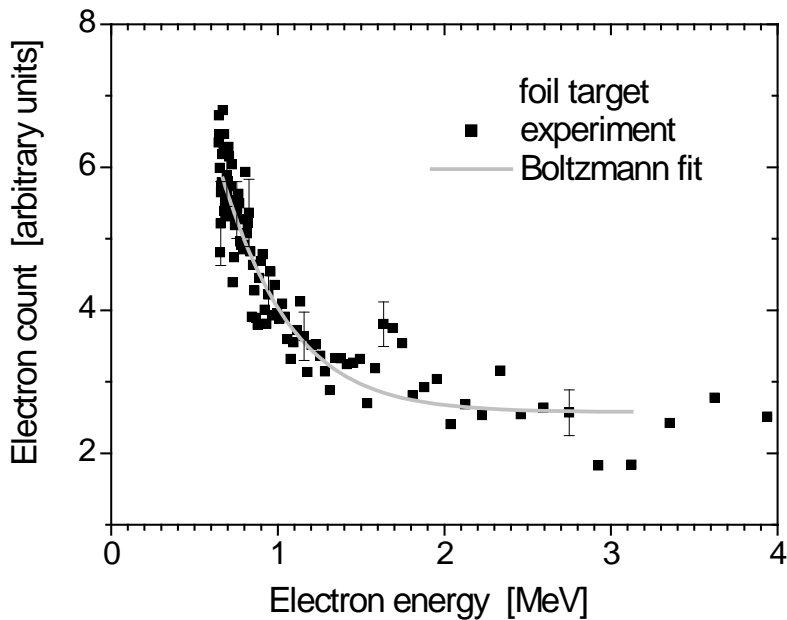

Fig. 7.5 Spectrum of fast electrons measured in the forward laser direction for irradiation of 25 μm foil targets with P laser polarization.
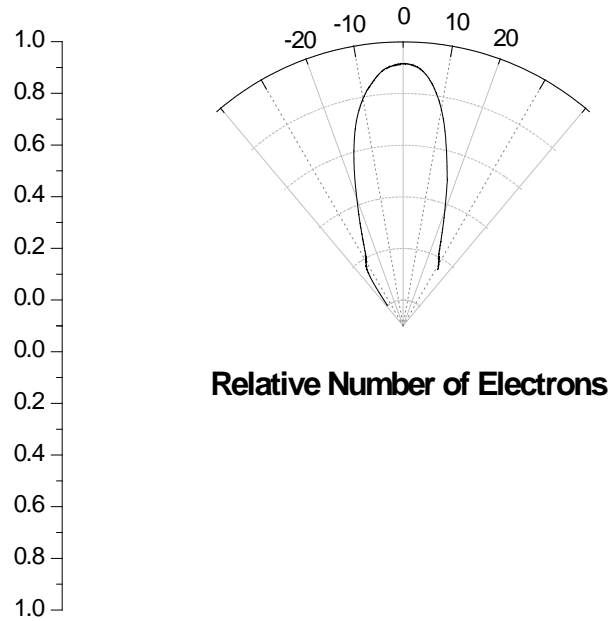
Fig. 7.6 The angular distribution relative to the laser forward direction of the energetic electrons emitted from a wire target. The raw film image is shown at the bottom of the figure.

INTERPRETATION OF ELECTRON ENERGY SPECTRA

The energy spectrum of hot electrons generated by ultrashort laser pulses is usually well described by a Boltzmann distribution with an effective temperature T_h. For electrons generated by ponderomotive acceleration, and laser intensity between 10^{18} and 10^{19} W/cm^2, this temperature is related to the ponderomotive potential by[18]

$$k_B T_h = m_0 c^2 (\sqrt{1 + I\lambda^2 [W/cm^2 \ \mu m^2]/1.38 \cdot 10^{18}} - 1).$$

(1)

For $I = 3\times10^{18}$ W.cm^2, and $\lambda = 0.8$ μm, the predicted temperature is 273 keV. The electron temperatures were estimated by fitting experimental spectral data to a Boltzmann distribution

$$f(E) = \frac{dN}{dE} \sim \frac{E^{\frac{1}{2}}}{T_h^{\frac{3}{2}}} \exp(-\frac{E}{kT_h})$$

(2)

in the range between 500 keV and 1 MeV. Figure 7 compares the results of the Boltzmann fits of the spectra in Figs 3-5 to the ponderomotive scaling, $T_h = 273$ keV. The fitted electron temperature for the foil target experiments (329 keV) agrees well with the ponderomotive value. For wire targets, the fitted electron temperature is substantially lower.

The data obtained from wire targets also exhibits polarization dependence. The fitted temperatures are 205 keV for laser P polarization and 174 keV for S polarization in the case of wire targets. These polarization differences may be related to the appearance of additional mechanisms such as resonance absorption. For wire targets with width smaller than the diameter of the laser spot, the laser electric field has a non-zero component perpendicular to the target at normal incidence, and resonance absorption may occur during the irradiation. This process may contribute to the increase in the number of electrons in the case of a P polarized laser beam. Alternatively, a mechanism known as Brunel (or vacuum) heating may be more efficient for energetic electron generation in the case of P polarization. In Brunel heating the electrons are pulled into vacuum in one half-cycle of the laser field, accelerated in vacuum, and re-injected into the dense region and farther into the target in the next half-cycle. In the case of a wire target, it may be possible that electrons that are pulled from the sides of the wire will subsequently be accelerated away from the target.
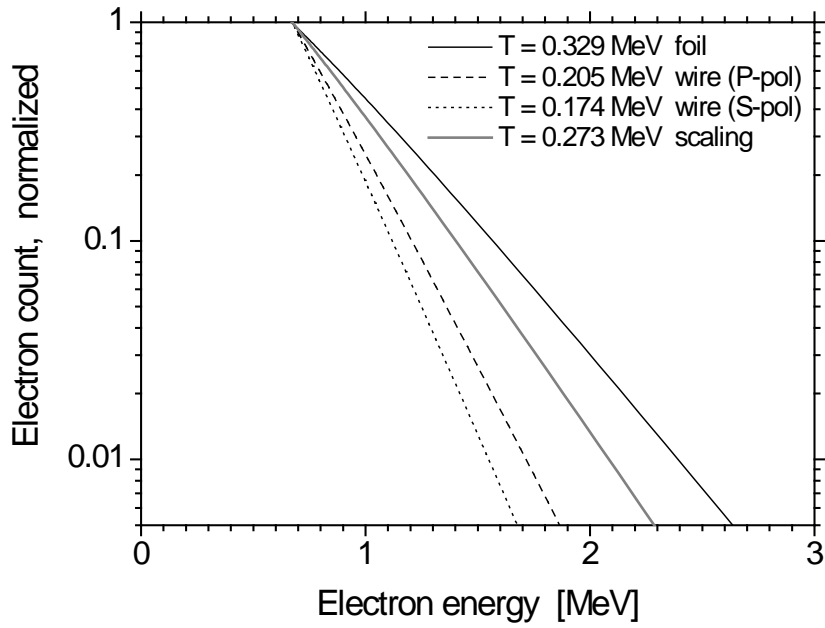
Fig 7.7 Normalized Boltzmann fit to the energy spectra of the electrons emitted from wire targets for P and S laser polarization, foil target

TRANSPORT OF ELECTRONS THROUGH A CAPILLARY DISCHARGE

In order for a capillary discharge to be suitable for a channel-guided LWFA, energetic electrons must be injected into the capillary with high efficiency and transported without substantial losses. The electrical current in the discharge produces substantial magnetic fields that can affect electron trajectories both inside and outside the capillary. For the LWFA parameter regime, the electromagnetic fields produced by the laser plasma interaction are generally much larger than the discharge fields. However, the fringing magnetic fields in the region just outside the discharge could deflect the externally-injected electrons and cause them to be lost. This problem was recently examined theoretically by us and concluded that for typical LWFA parameters, the deflection of injected electrons by the magnetic field of the discharge should be small compared with the acceptance of the wakefield.

A series of shots was taken in which electrons from a wire target were injected into a capillary discharge. The polarity of the discharge current was chosen such that the magnetic field inside the capillary confined the electrons. The standoff distance between the wire and the entrance to the capillary was 500 μm. The average number

26

of electrons transported through the capillary was 1.5×10^6 when the capillary current was triggered. When no discharge current was triggered, the capillary acted as a simple collimator, and the average number of electrons transported was actually slightly lower (1.4×10^6). These results are consistent with our theoretical model and suggest that there were not significant losses due to magnetic fields outside the capillary.

SIMULATION OF BEAM INJECTION INTO A CHANNEL-GUIDED LWFA

In this section, we will examine the evolution of a beam of electrons with a broad energy distribution in a channel guided LWFA. This analysis includes results from both analytic, one-dimensional Hamiltonian, and simulation using the two-dimensional laser propagation code WAKE. We show that an electron distribution that is consistent with the experimental results presented above can provide a useful electron injection bunch for an all-optical LWFA, and we will discuss the implications for future LWFA demonstration experiments.

We begin with the Hamiltonian function for an electron in a one-dimensional plasma wakefield of magnitude ϕ_0 in the frame moving with the wake[3,21,28]

$$H(\gamma,\psi) = \gamma \left(1 - \beta_g \beta\right) m_e c^2 + q \phi_0 \sin \psi \qquad (3)$$

where $\gamma = 1/\sqrt{1-\beta^2}$ is the electron Lorentz factor, $\beta = v_e/c, \beta_g = 1 - \omega_0^2/2\omega_p^2 - \lambda^2/2\pi^2 r_0^2$ is the laser group velocity normalized to c, including the finite spot size correction,[3,28-30] $\omega_p^2 = 4\pi q^2 n_e/m_e$ is the plasma frequency, q and m_e are the electron charge and mass, n_e is the plasma density and ω_0, λ, and r_0 are the laser frequency, wavelength and spot size of the laser pulse, respectively. This Hamiltonian can be used to get the electron equations of motion for the normalized momentum, $\mathbf{p} = \mathbf{p}_e/mc$, and phase, ψ, with respect to the acceleration distance, which we take to be the z direction. These equations are

$$\frac{d\mathbf{p}}{dz} = \phi_0 \left(\frac{\omega_p}{v_g} \right) \sqrt{1 + \frac{1}{\mathbf{p}^2}} \cos\psi$$

(4a)

$$\frac{d\psi}{dz} = \frac{\omega_p}{c} \left(\frac{1}{\beta_g} - \sqrt{1 + \frac{1}{\mathbf{p}^2}} \right).$$

(4b)

This one dimensional analysis neglects the effects of the transverse electric field, which for an ideal wake in a uniform plasma is sinusoidal and $\pi/2$ out of phase with respect to the axial field. For this ideal case, it is often assumed that only electrons whose phase always that remains between 0 and π experience a focusing transverse field, while those that move out of this range of phases are expelled. Only those phases between π and $\pi/2$ are both focusing and accelerating. However, a more careful examination of the wakefields in the presence of a plasma channel reveals that the range of phases that are both focusing and accelerating is significantly larger than in the ideal uniform plasma case. The simulations that we have performed show that there is an increased working phase in the channel-guided simulations of approximately $\pi/6$.

The expected energy gain may be estimated by integrating Eqs. (4a,b). The initial energy and phase of the electron is chosen to be on the lowest energy phase space orbit whose phase is never smaller than $-\pi/6$, which thus includes the expansion of the focusing region described in the previous paragraph. The dashed curve in Fig. 8 shows the normalized momentum for the accelerating electron as a function of z for a case with normalized potential $\phi_0 = 0.45$ and $\omega_0/\omega_p = 50$. The accelerated electrons reach their maximum energy after propagating a distance of 4 cm, which is nearly identical to the classic dephasing length[3,5-7] $L_d = \lambda_p / 4(1 - \beta_g)$.

Also in Fig. 7.8 are the results from a standard LWFA WAKE test particle simulation with (FWHM) pulse length $\tau_L = 67$ fsec, peak laser pulse power $P_0 = 10$ TW, and injected laser spot size $r_0 = 15$ μm. The on-axis density of the plasma channel was $n_0 = 7 \times 10^{17} \text{cm}^{-3}$, with a parabolic channel density profile chosen so that the equilibrium spot size r_M was equal to r_0. As in similar simulations reported in the past, this "matched" injection with an ideal plasma channel resulted in a laser

pulse that propagated at nearly constant spot size and generated a well-defined wakefield whose maximum amplitude was nearly constant. The initial test particle distribution was a one sided Maxwell-Boltzmann thermal distribution with a 250 KeV temperature, located at 1.0 radian in phase, with a 21 fs electron bunch. The electron momentum from the simulation includes error bars that represent the standard deviation of the electron momentum for the bunch. Notice that initially this momentum spread is relatively small and constant; however, after about 2.5 cm the energy spread begins to increase rapidly.

This dynamic in the accelerating behavior of the electrons can be understood as follows. Consider two electrons that are initially at the same phase in the accelerating structure with one electron having the minimum energy to be captured and the other electron having somewhat more energy. As the electrons accelerate, the higher energy electron will reach the de-phasing limit for acceleration sooner than an electron with lower energy due to the difference in relative slippage between the electrons and the laser pulse group velocity. Therefore, as the electrons continue lower energy electron continues to accelerate the electron that has reached the de-phasing limit will begin to decelerate, thus increasing the energy spread of the electron bunch. This process is clearly evident in the rapid increase in the momentum spread after 2.5 cm. This process provides for a relatively small momentum spread at the location where the first electrons reach their de-phasing limit.

This reduced energy spread can be seen in Fig. 7.9, which presents axial phase space results from the WAKE simulation discussed above. The initial particle distribution, in the lower left corner and momentum referenced to the left axis, was the one sided Maxwell-Boltzmann thermal distribution described previously. The electron distribution in the upper right corner, with momentum values referenced to the right axis, is for the electron bunch after approximately 2.5 cm of acceleration. The total energy gain is approximately 600 MeV with a relative energy spread of 3 percent. The electron bunch has also undergone phase compression to 0.25 radians, ~5 fs. Based on both the analytic and simulation results we conclude that it is possible to use the broad electron energy distribution provided from a wire target for interesting and useful exploration of LWFA schemes, particularly if large numbers of electrons can be produced with a simple experimental geometry. These results also demonstrate that as the propagation distance approaches the dephasing length, there is a substantial increase in the energy spread.
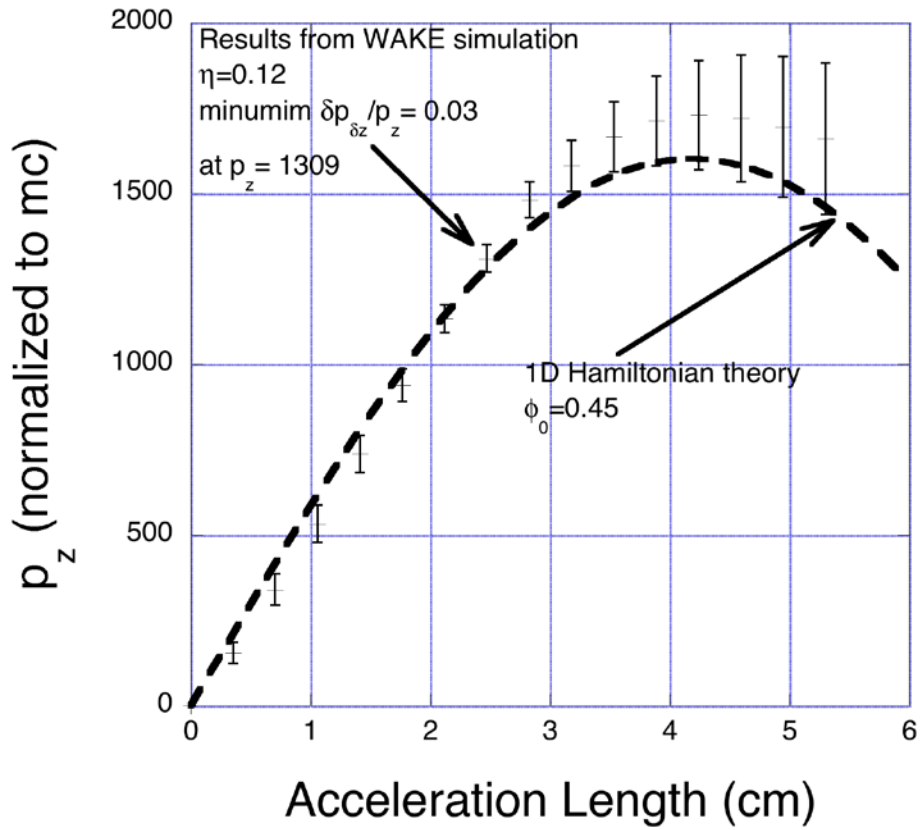
Fig 7.8 Average momentum for the accelerating electrons as a function of acceleration length for both a test particle simulation using WAKE and the trajectories based on the one-dimensional Equations of Motion.
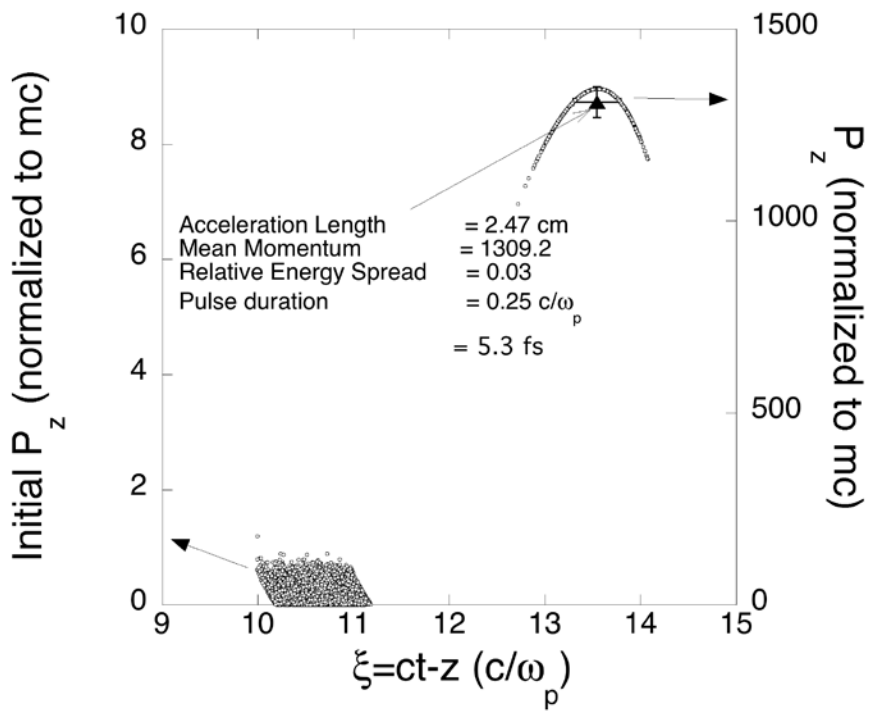
Fig 7.9 Test particle axial phase space distributions for the initial and optimal, e.g., minimum relative energy spread, times during the WAKE simulation.

CONCLUSIONS (related to the electron propagation through capillary channel).

Electron bunches with energies up to several MeV were generated by irradiating tungsten wires with 45 fs, 10^{18} W/cm^2, 10 Hz laser pulses. The energetic electron yield was about 1.5×10^6 per pulse into a 20° cone. This energetic electron bunch may be used as an optical injector for a channel-guided laser wakefield accelerator. The proposed method provides the possibility of simplified timing between injection and acceleration. Although the initial energy spread in the charge bunch is substantial, simulation studies demonstrate that it may be possible to produce a high-quality, ultrashort, accelerated beam bunch with an energy spread of only a few percent. These favorable results are due to a combination of pruning of particles at unfavorable phases or initial energies, rapid acceleration, and strong phase bunching.

The average number of electrons transported through the capillary was same when the capillary current was triggered or when no discharge current was triggered and the capillary acted as a simple collimator. These results are consistent with our theoretical model and suggest that there were not significant losses due to magnetic fields outside the capillary.

8. <u>Staged all-optical laser wakefield acceleration.</u>

Prior to the staging of the capillary based accelerators, we performed a proof-of-principal experiment on staged optical injection and laser wakefield acceleration using two different short laser pulses focused into two spatially separated gas jets. We recently finished analyzing important results from this experiment.

The first gas jet was used as an injector and the second one as the accelerator. Both the injector and the accelerator operated in the SM-LWFA regime, but in different trapping conditions. Relative amplitudes of the acceleration wakefields was measured by forward Raman scattering (FRS). Strong dependence of the electrons energy gain on the timing between the injection and acceleration laser beams, and the
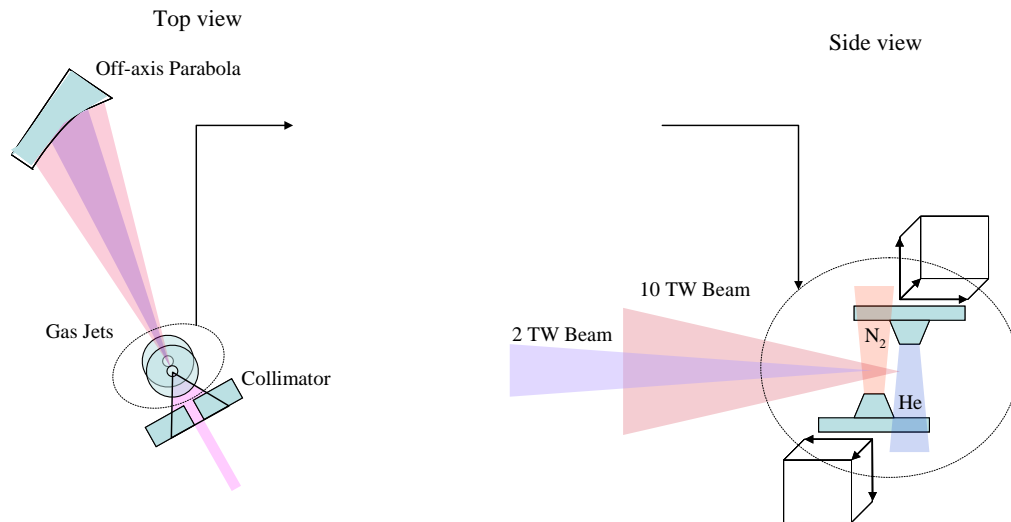

Figure 8.1: Experimental setup for staged all-optical injection acceleration experiment.

time difference between the occurrence of the maximum number of accelerated electrons and the peak FRS clearly identified the acceleration of injected electrons.

The NRL T-cubed laser system at a wavelength of 1054 nm was used for the experiment [C. I. Moore, A. Ting, T. Jones, E. Briscoe, B. Hafizi, R. F. Hubbard, and P. Sprangle, Physics of Plasmas, 8, 2481 (2001).]. The stretched beam from the chirped pulse amplification laser system was split before it reaches the final amplifier. The first beam containing most of the energy was sent through an adjustable delay line and then compressed in air. This laser beam (2 TW, 500 fs, 1 J) was focused into a nitrogen gas jet (5×10^{18} cm^{-3} neutral density) using a 32 cm focal length (F#10 for this beam) off-axis parabola (Fig. 1). The adjustable delay line allowed setting the timing between the laser pulses. The nitrogen gas jet has a cross sectional diameter of about 500 μm. The laser intensity of the 2 TW beam at focus was about 3×10^{17}

W/cm^2 in vacuum. During the alignment procedure the position of the gas jet was adjusted in order to generate the highest energy electrons. In the laser-plasma interaction, the nitrogen gas was up to five times ionized resulting in a plasma density of 3x 10^{19} cm^{-3}. The 2 TW laser beam and the nitrogen gas jet are being used as the injector.

The second laser beam was sent through an additional amplifier, a spatial filter (1:1.7 beam expansion) and then compressed in vacuum, resulting in a 10 TW (5 J, 500 fs) output laser beam. After recombining collinearly with the first beam by using a thin-film polarizer and a half-wave plate, the second beam was focused by the same off-axis parabola (F#6 for this beam) into a helium gas jet that was separated by 0.5 mm downstream from the nitrogen jet (Fig. 8.1). To separate the focal spots of the two laser beams, we changed the collimation of the 10 TW beam by adjusting the output lens of the spatial filter. Shifting the lens toward the spatial filter makes the beam slightly diverging and as a result shifts the focal spot farther. The focal spot positions of both lasers were fixed by the external optics. Measurements of the positions of laser sparks at very low intensities showed that the focal spot separation was 500 microns. The helium gas jet has a diameter of 1.5 mm and the neutral gas density was 5x10^{18} cm^{-3}. The peak laser intensity of the 10 TW beam was about 3x10^{18} W/cm^2 as measured in vacuum. The propagation of the laser beam through the nitrogen gas or plasma could aggravate the coupling of the laser in the helium gas jet and reduce the peak intensity. During the laser-plasma interaction, the helium was fully ionized resulting in a plasma density of 1x10^{19} cm^{-3}. The 10 TW beam and the helium gas jet are being used as the accelerator. The position of the helium gas jet was adjusted to generate the highest energy electrons. The gas flow of the helium gas jet overlaps with the nitrogen gas jet and since they were ejected in opposite directions (fig. 1), there was a sharp boundary separating the two gas regions.
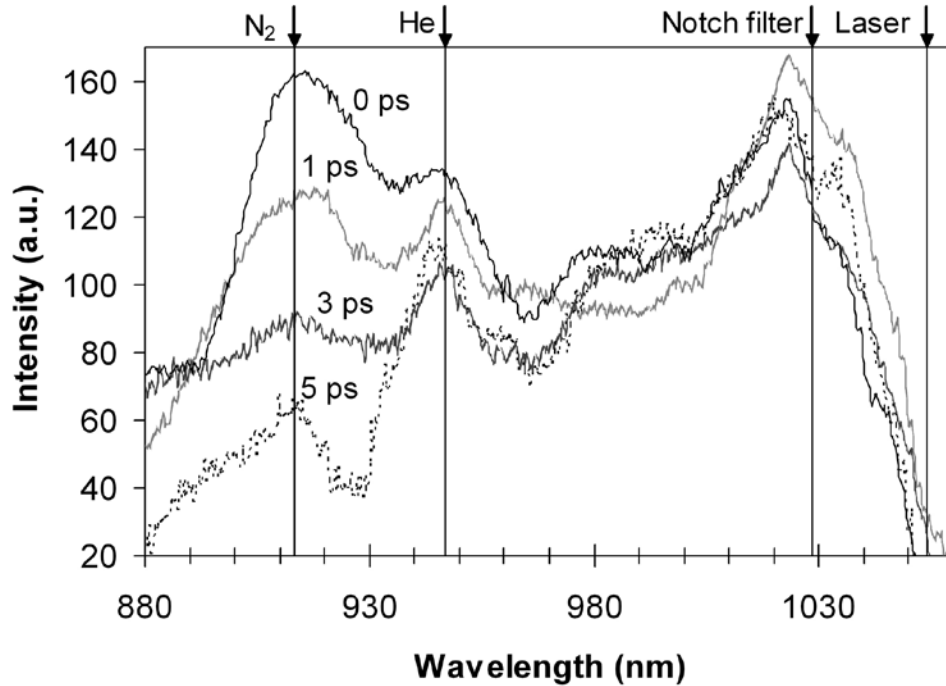
Figure 8.2: Evolution of the FRS spectra of the 10 TW beam as function of delay between the 10 TW and 2 TW laser beams. After 6 ps delay the nitrogen peak disappears.

About 4% of the 2 TW laser beam intensity was reflected from the thin-film polarizer and sent through a doubling crystal and an adjustable delay line. This frequency doubled laser beam was aligned to pass through the gas jets transversely and was used as a probe in a Schlieren shadowgraphy diagnostic. This allowed initial sub-picosecond synchronization and 10 micrometer spatial alignment of the two laser beams. Using this diagnostic we tested the precision of the adjustable delay between the two laser beams to better than 100 fs timing. The first anti-Stokes forward Raman scattering spectra was measured by collecting the emission light at 10 degrees with respect to the direction of the laser beam propagation. Divergence and polarization difference between the 2 TW and 10 TW laser beams allowed the separation of the FRS signals of the beams. The difference in the plasma densities of the two gas jets also makes it possible to further separate the FRS signals from the nitrogen and the helium plasmas. In this experiment, we only analyzed the FRS spectra of the 10 TW acceleration beam. Figure 8.2 shows the evolution of the 10 TW FRS spectra as a function of the time delay between 2 TW and 10 TW laser beams. The nitrogen

plasma peak decays with the delay as expected. The helium plasma peak remains constant to within shot to shot fluctuations.

Accelerated electrons that are generated in the gas jets, passed through a collimator with a 3 mm aperture (F#30) and an integrating current transformer (ICT) for absolute calibration of the number of injected and accelerated electrons. The minimum resolvable charge of the ICT is about 6 pC, with an input current rise time <1 ps. The selected electrons were sent into an electron spectrometer which consists of a sector electro-magnet and a 14 cm long plastic scintillator (1 mm BC-400). The front side of the scintillator is covered with 2 layers of 6 μm aluminum foil to block the ambient light and to attenuate the number of low energy electrons. The back side of the scintillator was imaged onto a gated optical intensifier. This allowed a single shot electron energy spectrum to be measured. Energy calibration of the electron spectrometer was obtained using a 3D ray-tracing code [D. F. Gordon, CyberRay electron propagation code (Icarus Research Inc., Bethesda, MD, 2003)].

In our previous experiments [A. Ting, D. Kaganovich, D. F. Gordon, R. F. Hubbard, and P. Sprangle, Phys. of Plasmas **12**, 010701 (2005)] we used single laser beam and single gas jet to study the properties of the injected electrons. The maximum electron energy detected in this experiment using the same electron spectrometer was around 8 MeV using a laser intensity that was 3 times higher (10^{19} W/cm^2) and a better coupling between the laser and the gas jet. In present experiment we deliberately configured the coupling between the 10 TW beam and the He gas jet to be sub-optimized for self-trapping and acceleration of background plasma electrons. The focusing of the 10 TW beam was affected by both its positioning with respect to the helium nozzle and its passage through the nitrogen plasma.

3. Analysis of the experimental results.

Figure 3 shows the single shot electron energy spectra of the injected and accelerated electrons. The solid line in figure 8.3 is the noise floor. It was determined by studying the positron side of the scintillator, where we observe that the x-ray background is uniform across the scintillator. To determine the noise floor in units of electrons per MeV, this constant background was processed exactly the same way as the electron data. The maximum energy of the injected electrons was below 0.5 MeV. It was measured by firing the 2 TW beam and the Nitrogen gas jet only. Turning on

the Helium gas jet had no effect on this spectrum. The electron energy spectrum shown in figure 3(b) represents accelerated electrons at the optimum time delay between the injection and acceleration laser beams showing electrons well above 20 MeV. For this shot, both gas jets and both laser beams were fired. It is possible that even higher energy electrons were generated in this and similar shots, but the number of these electrons was below the noise detection level. We performed the following null tests: 1) By firing only the acceleration (10 TW) laser beam and both gas jets, we detected no electrons signal, apparently because of ionization defocusing of the laser beam in the nitrogen gas jet; 2) Firing the 10 TW laser (with or without 2 TW beam) directly into the helium gas jet with the nitrogen jet being off generated electrons of about 1 MeV only; 3) Firing both laser beams into the nitrogen jet with the helium jet being off generated electrons below 1 MeV. All these tests indicated that the high energy electrons were not from self trapping of the background plasma electrons.
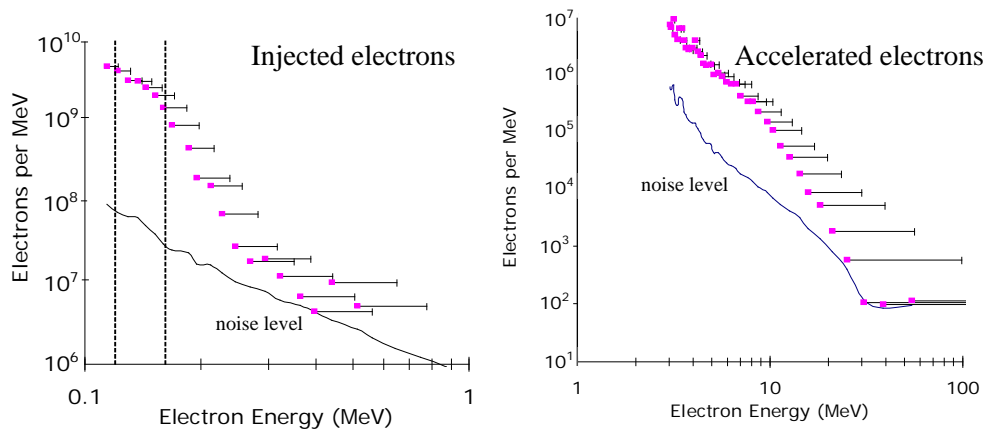
Figure 8.3: Injection and acceleration electrons energy spectrum. About 0.3% of the electrons between dotted lines on the injection spectrum get trapped and accelerated to more than 10 MeV.

By changing the time delay between the injection and acceleration laser beams as shown in figure 8.4, we observed that the high energy electrons (> 10 MeV) appear in a very narrow time window of 3 ps. Note that even though each point on the graph represents a single shot, the data was repeatable under the same conditions. The vertical error bars were estimated from the experimental errors. Also shown in figure 4 is the amplitude of the FRS signal (taken as peak value of FRS in figure 2) from the 10 TW laser beam seeded and modulated by the nitrogen plasma. Despite the well

correlated behavior between the number of the high energy electrons and the FRS signal, there is one crucial difference. Figure 8.4 shows that the largest number of high energy electrons appeared at 1 ps (± 100 fs) delay of the acceleration beam after injection beam, while the highest FRS signal is generated when the two beams are fired at the same time. The peak FRS signal is expected to appear at zero delay and therefore provided a confirmation of the time measurement accuracy of the Schlieren shadowgraphy diagnostic. Taking into account the fact that the injection electrons need some time to propagate the 0.5 mm distance between the injector and the accelerator at a speed that is below the speed of light, this 1 ps time delay provides the proof that the accelerated electrons were in fact the injected electrons. These electrons can be estimated to have a ~150 keV in energy so that they require the extra 1 ps to propagate the 0.5 mm distance to catch up with the laser beam. This energy of the injected electrons agrees with the energy spectrum shown in figure 8.3(a). Although the injector produces about 3×10^{8} of such electrons [between dotted lines on fig. 8.3(a)], only about 0.3% was trapped and accelerated. This reduction occurs not only because exact phasing in time (1/4 cycle of the plasma period) is required [14], but also for the fact that the relatively low energy electrons could be trapped only by the few most dominant wakefield periods (among the total of many tens of periods) in the acceleration stage. Higher energy electrons probably were also trapped and accelerated. However, as it was shown in figure 8.3(a), the number of these electrons decreases rapidly as the energy increases. That could explain why the number of high energy electrons at 0-time delay is much lower than the number of similar electrons at the 1 ps delay in figure 8.4.
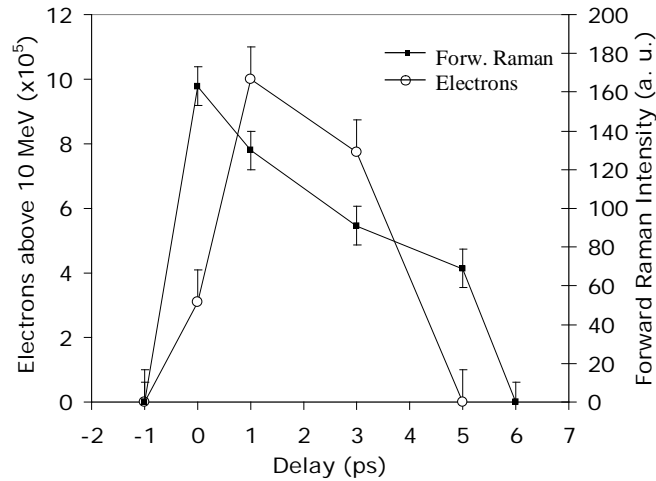
Figure 8.4: First anti-Stokes forward Raman intensity (solid squares) and the number of electrons above 10 MeV (open circles) as function of delay time between injection and acceleration laser beams. The data points of the number of electrons are represented at the lower bound of the number estimates with the error bars extending to higher possible numbers.

The accelerated electrons were not originated as self-trapped plasma electrons in the self-modulated wakefield of the 10 TW beam. Since the 10 TW beam is not focused in the nitrogen but reaches high intensities only at the far end of this gas jet, it could not have developed sufficient modulations in the nitrogen plasma and must be seeded by the wakefield of the 2 TW beam. However, this seeding can not contribute to the wakefield in the helium acceleration stage, because the modulation on the 10 TW laser beam by the nitrogen plasma does not match the helium plasma density which is 3 times lower. Similar seeding by the 2 TW beam in the helium plasma did not occur because the 2 TW laser beam has already defocused there. In fact, the FRS from the helium was observed to be lower than that from the nitrogen (zero time spectra in figure 8.2). Therefore relatively weak wakefield was generated in the acceleration stage and it was not strong enough to pick up and accelerate any background electrons to high energies. The short time window of the nitrogen FRS signal in figure 2 also indicates that the lifetime of the self-modulated wakefield created by the 2 TW beam in nitrogen is about 6 picoseconds similar to previously reported experiments [A. Ting, K. Krushelnick, C. I. Moore, H. R. Burris, E. Esarey, J. Krall, and P. Sprangle, Phys. Rev. Lett., **77**, 5377 (1996); S. P. Le Blanc, M. C.

Downer, R. Wagner, S.-Y. Chen, **A.** Maksimchuk, G. Mourou and D. Umstadter, Phys. Rev. Lett., **77**, 5381 (1996)]. Theoretically the sharp plasma density gradient between the helium and nitrogen plasmas could perturb the phase space of the background oscillating plasma electrons sufficiently to trigger injection into the plasma wakefield that passes through the boundary [H. Suk, N. Barov, and J. B. Rosenzweig, and E. Esarey, Phys. Rev. Lett., **86**, 1011 (2001)]. However, since the plasma and thus the sharp boundary could persist for much longer time than a few picoseconds, we would not have observed the short time dependence shown in this experiment.

In our previous experiment [A. Ting, D. Kaganovich, D. F. Gordon, R. F. Hubbard, and P. Sprangle, Phys. of Plasmas **12**, 010701 (2005)] we found that divergence of the injected electrons is large. Acceptance angle of the acceleration stage is also wide [B. Hafizi, D. F. Gordon, A. Zigler, A. Ting, Physics of Plasmas, **10**, 2545 (2003)]. However the high energy electrons appeared only at the perfect alignment between the laser beams. A 10 μm misalignment between the focal spots (measured by two telescopes) decreased the number of high energy electrons to undetectably low level. This high sensitivity is a result of ponderomotive expulsion of misaligned electrons by the 10 TW laser beam. As the injected electrons propagate from the first to the second jet, they are overtaken by the 10 TW laser pulse, and are exposed to a large radial ponderomotive force. The ponderomotive potential for an electron is

$$F = \frac{a^2}{4\sqrt{mc^2\left(1 + \frac{a^2}{2}\right)}}$$

where a is the peak normalized vector potential and m electron mass. Between the two jets the 10 TW pulse is nearly focused so that a is about unity and the ponderomotive potential is about 100 keV. For the low energy injection electrons, the velocity gained in passing through the ponderomotive potential can be approximated by

$$v \approx \sqrt{\frac{2F}{m}} \ .$$

The characteristic time for this to occur can be found from

$$mv = \frac{Ft}{r}$$

where r is the laser spot size and t is the characteristic time. This gives

$$t = r\sqrt{\frac{2m}{F}}$$

For a 10 micron spot size the characteristic time is about 100 fs. This corresponds to about 15 microns of propagation for the 100 keV injection electrons. Thus, in a distance short compared to the separation between the two jets, the injection electrons can be deflected into a large angle and miss the accelerating structure entirely. Only particles very close to the laser axis, where the ponderomotive force vanishes, can survive. From our experiment, all it took was a 10 microns mis-alignment measured at the source of the injected electrons, i. e. the nitrogen jet, to foul the injection.

REFERENCES

1. T. G. Jones, A. Ting, D. Kaganovich, C. I. Moore, and P. Sprangle, Phys. Plasmas **10**, 4504 (2003).
2. Plexiglas Sunactive ® GS, Product description www.plexiglas.de
3. B. Greenberg, M. Levin, A. Pukhov, and A. Zigler, Appl. Phys. Lett. **83**, 2961 (2003).
4. H.R. Griem, *Spectral Line Broadening by Plasmas* (Academic Press, New York, 1974).
5. S. A. Flih, E. Oks, and Y. Vitel, Phys. B. At. Mol. Opt. Phys. **36**, 283 (2003).
6. S. P. Nikitin, T. M. Antonsen, T. R. Clark, Y. Li, and H. M. Milchberg, Optics. Lett. **22**, 1787 (1997).
7. D. F. Gordon, R. F. Hubbard, J. H. Cooley, B. Hafizi, and P. Sprangle, Phys. Rev. E **71**, 026404 (2005).
8. R. F. Hubbard, D. F. Gordon, J. H. Cooley, B. Hafizi, T. G. Jones, D. Kaganovich, P. Sprangle, A. Ting, and A. Zigler, IEEE Trans. Plasma Sci. **33**,712 (2005).
9. D. Strickland and G. Mourou, Opt. Commun. **56**, 219 (1985).
10. T. Tajima and J.M. Dawson, Phys. Rev. Lett. **43,** 267 (1979).
11. E. Esarey, P. Sprangle, J. Krall, and A. Ting, IEEE Trans. Plasma Sci. **24**, 252 (1996) and references therein.
12. P. Sprangle, E. Esarey, A. Ting, and G. Joyce, Appl. Phys. Lett. **53**, 2146 (1988); L. M. Gorbunov and V. I. Kirsanov, Sov. Phys. JETP **66**, 290 (1987).
13. R. F. Hubbard, D. Kaganovich, B. Hafizi, C. I. Moore, P. Sprangle, A. Ting and A. Zigler, Phys. Rev. E **63**, 036502 (2001); P. Sprangle, B. Hafizi, J. R. Peñano, R. F. Hubbard, A. Ting, C. I. Moore, D. F. Gordon, A. Zigler, D. Kaganovich and T. M. Antonsen, Phys. Rev. E **63**, 056405 (2001).
14. W. P. Leemans, C. W. Siders, E. Esarey, N. E. Andreev, G. Shvets, and W. B. Mori, IEEE Trans. Plasma Sci. **24**, 331 (1996).
15. F. Amiranoff, S. Baton, D. Bernard, B. Cros, D. Descamps, F. Dorchies, F. Jacquet, V. Malka, J. R. Marquès, G. Matthieussent, P. Miné, A. Modena, P.

Mora, J. Morillo, and Z. Najmudin, Phys. Rev Lett. **81**, 995 (1998); F. Dorchies, F. Amiranoff, V. Malka, J. R. Marques, A. Modena, D. Bernard, F. Jacquet, Ph. Mine, B. Cros, G. Matthieussent, P. Mora, A. Solodov, J. Morillo, and Z. Najmudin, Phys. Plasmas **6**, 2903 (1999).

16. Modena, Z. Najmudin, A. E. Dangor, C. E. Clayton, K. A. Marsh, C. Joshi, V. Malka, C. B. Darrow, and C. Danson, IEEE Trans. Plasma Sci. **PS-24**, 289 (1996); D Gordon, K. C. Tzeng, C. E. Clayton, A. E. Dangor, V. Malka, K. A. Marsh, A. Modena, W. B. Mori, P. Muggli, Z. Najmudin, D. Neely, C. Danson, and C. Joshi, Phys. Rev. Lett. **82**, 2133 (1998).

17. C. Gahn, G. D. Tsakiris, G. Pretzler, K. J. Witte, P. Thirolf, D. Habs, C. Delfin, and C. G. Wahlström, Phys. Plasmas **9**, 987 (2002).

18. C. I. Moore, A. Ting, K. Krushelnick, E. Esarey, R. F. Hubbard, B. Hafizi, H. R. Burris, C. Manka, and P. Sprangle, Phys. Rev. Lett. **79**, 3909 (1997).

19. V. Malka, J. Faure, J.R. Marque, F. Amiranoff, J. P. Roussseau, S. Ranc, J. P Chamberet, Z. Najmudin, B. Walton, P. Mora, and A. Solodov, Phys. Plasmas **8**, 2605 (2001).

20. D. Giulietti, M. Galimberti, A. Giulietti, L. A. Gizzi, M. Borghesi, Ph. Balcou, A. Rousse, and J. Ph. Rousseau, Phys. Rev E **64**, 015402 (R) (2001).

21. D. Umstadter, J.K. Kim, and E. Dodd, Phys. Rev. Lett. **76**, 2073 (1966).

22. E. Esarey, R.F Hubbard, W.P. Leemans, A. Ting, and P. Sprangle, Phys. Rev. Lett. **79**, 2682 (1997).

23. C. I. Moore, A. Ting, S. J. McNaught, J. Qiu, H. E. Burris, and P. Sprangle, Phys. Rev. Lett. **82**, 1688 (1999).'

24. P.V. Nickles, M.P. Kalachnikov, P.J. Warwick, K. A. Janulewicz, W. Sadner, U. Jahnke, D. Hilscher, M. Schnürer, R. Nolte, and A. Rousse, Quantum Electron **29**, 444 (1999).

25. K. Nakajima, D. Fisher, T. Kawakubo, H. Hashaniki, A. Ogata, Y. Kato, Y. Kitagawa, R. Kodama, K. Mima, H. Shiraga, K. Suzuki, K. Yamakawa, T. Zhang, Y. Sakawa, T. Shoji, Y. Nishida, N. Yagami, M. Downer, and T. Tajima, Phys. Rev. Lett. **74**, 4428 (1995).

26. G. Malka and J.L. Miquel, Phys. Rev. Lett. **77**, 75 (1996).

27. Y. Ehrlich, A. Zigler, C. Cohen, J. Krall, and P. Sprangle, Phys. Rev. Lett. **77**, 4186 (1996).

28. C.G. Durfee and H.M. Milchberg, Phys. Rev. E **71**, 2409 (1993)

29. R. F. Hubbard, D.F. Gordon, T. Jones, J.R. Peñano, P. Sprangle, A. Ting, B. Hafizi, A. Zigler, and D. Kaganovich, in *Proceedings of the 2003 Particle Accelerator Conference*, (Institute of Electrical and Electronics Engineers, Piscataway, NJ, 2003), p. 716.

30. P. Mora. and T.M. Antonsen, Phys. Plasmas **4**, 217 (1997)

31. S. C. Wilks, W. L. Kruer, M. Tabak, and A. B. Langdon, Phys. Rev. Lett. **69**, 1383 (1992).

32. S.C. Wilks and W.L. Kruer, IEEE J. Quantum Electron. **33**, 1954 (1997).

33. F. Brunel, Phys. Rev. Lett. **59**, 52 (1987).

34. B. Hafizi, D. F. Gordon, A. Zigler, and A. Ting, Phys. Plasmas **10**, 2545 (2003).

35. E. Esarey. and M. Pilloff, Phys. Plasmas **2**, 1432 (1995).

36. N. E. Andreev, L. M. Gorbunov, V. I. Kirsanov, K. Nakajima, and A. Ogata, Phys. Plasmas **4** 1145 (1997).

37. W. D. Kimura, M. babzien, I. Ben-Zvi, L. P. Campbell, D. b. Cline, C. E. Dilley, J. I. V. Pogorelsky. D. C. Quimby, J. Skaritka, L. C. Steinhower, V. Yakimenko, and F. Zhou, Phys. rev. Lett. **92**, 054801 (2004).

Publications

1. A. Ting, D. Kaganovich, D.F. Gordon, R.F. Hubbard, and P. Sprangle, "Generation and Measurements of High Energy Injection Electrons from the High Density Laser Ionization and Ponderomotive Acceleration", Phys. Plasmas <u>12</u>, 010701 (2005).

2. R. F. Hubbard, D. F. Gordon, J. H. Cooley, B. Hafizi, T. G. Jones, D. Kaganovich, A. Ting, A. Zigler, and J. Dexter, "Trapping and Acceleration of Nonideal Injected Electron Bunches in Laser Wakefield Accelerators," IEEE Trans. Pl. Sc. <u>33</u>, 712 (2005).

3. D. F. Gordon, R. F. Hubbard, J. H. Cooley, B. Hafizi, and P. Sprangle, "Quasi-monoenergetic Electrons from Unphased Injection Into Channel Guided Laser Wakefield Accelerators," Phys. Rev. E **71** 026404 (2005).

4. D. Kaganovich, A. Ting, D. Gordon, T. G. Jones, R. Hubbard and P. Sprangle, "Generation of high energy electrons in a double gas jet and laser wakefield acceleration", IEEE Trans. Pl. Sc. <u>33</u>, 735 (2005).

5. B. Hafizi, D.F. Gordon, A. Zigler, and A. Ting, "Electron Trajectories in Magnetic Field of Capillary Discharge: Application to Laser Wakefield Acceleration in Plasma Channel", Phys. Plasmas <u>10</u>, 2545 (2003).

6. T.G. Jones, A. Ting, D. Kaganovich, C.I. Moore, and P. Sprangle, "Spatially resolved interferometric measurement of a discharge capillary plasma channel", Phys. Plasmas <u>10</u>, 4504 (2003).

7. D. Kaganovich, A. Ting, D. Gordon, R.F. Hubbard, and P. Sprangle, "First Demonstration of a Staged Optical Injection and Laser Wakefield Acceleration", submitted to Phys. Plasmas, 2005.

8. D. F. Gordon, B. Hafizi, R. F. Hubbard, J. R. Peñano, P. Sprangle, and A. Ting, "Asymmetric Self-Phase Modulation and Compression of Short Laser Pulses in Plasma Channels," Phys. Rev. Lett. **90**, 215001 (2003).

9. B. Hafizi, P. Sprangle, J. R. Peñano, and D. F. Gordon, "Electron Distribution Function in Short-Pulse Photoionization," Phys. Rev. E **67**, 056407 (2003).

10. B. Hafizi, D. F. Gordon, A. Zigler, and A. Ting, "Electron Trajectories in the Magnetic Field of a Capillary Discharge: Application to Laser Wakefield Accelerators in Plasma Channel," Phys. Plasmas **10**, 2545 (2003).

11. S. Eisenmann, B. Greenberg, T. Palhan, A. Zigler, D. Kaganovich, R. F. Hubbard, J. Cooley, A. Ting, P. Sprangle, D. F. Gordon, M. Frankel, S. Maman, D. Fisher, and Z. Henis, "All Optical Injector Using an Intense Ultrashort Pulse Laser and a Solid Wire Target," submitted to J. Physics B, 2005.

12. A. Zigler, M. Levin, A. Pukhov, R. F. Hubbard, D .Kaganovich, D. F. Gordon, P. Sprangle, A. Ting, and B. Hafizi, "Longitudinal Profiles of Plasma Parameters in a Laser-ignited Capillary Discharge and Implications for Laser Wakefield Accelerator Applications," submitted to J. Apply. Phys., 2005.

Presentations and Conference Proceedings

a. A. Ting, D. Kaganovich , D. F. Gordon, R. F. Hubbard and P. Sprangle, "High Energy Injection Electrons From The High Density Laser Ionization And Ponderomotive Acceleration," the 11th Advanced Accelerator Concepts Workshop 2004, Stony Brook, NY, June 21-26, 2004 (invited talk); also to appear in workshop proceedings.

b. R. F. Hubbard, *et al.,* "Trapping and Acceleration of Nonideal Injected Electron Bunches in Channel-Guided LWFAs," Advanced Accelerator Concepts Workshop, June, 2004; also to appear in workshop proceedings.

c. J. H. Cooley, R. F. Hubbard, D. F. Gordon, A. Zigler, A. Ting, and P. Sprangle., "Effective Electron Beam Injection with Broad Energy Initial Beam," Advanced Accelerator Concepts Workshop, June, 2004; also to appear in workshop proceedings.

d. D. Kaganovich, A. Ting, D. Gordon, E. Briscoe, T. Jones, R. Hubbard and P. Sprangle, "Experimental Demonstration of a Staged Optical Injection and Laser Wakefield Acceleration," the 11th Advanced Accelerator Concepts Workshop 2004, Stony Brook, NY, June 21-26, 2004 (oral).

e. D. Kaganovich, A. Ting, D. Gordon, T.G. Jones, E. Briscoe, R. Hubbard, and P. Sprangle, "Optical Injection in a Laser Wake Field Accelerator," 2004 IEEE International Conference on Plasma Science, Baltimore, MD, June 28 – July 1, 2004 (oral).

f. A. Zigler, D. Kaganovich, B. Hafizi, M. Levin, B. Grenberg, A. Puhov, A. Ting, T. Jones, R.F. Hubbard, and P. Sprangle, "Guiding of Ultrahigh Laser Intensities in Ablative Capillary Discharge Plasma Channel with Laser Ignition," the 11th Advanced Accelerator Concepts Workshop 2004, Stony Brook, NY, June 21-26, 2004 (oral).

g. R. F. Hubbard, B. Hafizi, A. Ting, D. F. Gordon, T. G. Jones, D. Kaganovich, J. R. Peñano, P. Sprangle, and A. Zigler, "Focusing of Intense Laser Pulses Using Plasma Channels," in *Advanced Accelerator Concepts, 10th Workshop,* AIP Conference Proceedings 647 (American Institute of Physics, Melville, NY, 2002), p. 664.

h. B. Hafizi, *et al.,* "Design of a Multi-Stage LWFA in a Plasma Channel," 2003 Particle Accelerator Conference (Poster TPPG040).

i. R. F. Hubbard, D. F. Gordon, T. G. Jones, J. R. Peñano, P. Sprangle, A. Ting, B. Hafizi, A. Zigler, and D. Kaganovich, "Simulation of Accelerated Electron

Spectra in Laser Wakefield Accelerators," *Proceedings of the 2003 Particle Accelerator Conference*, p. 716.

j. A. Zigler, B. Greenberg, T. Palhan, D. Kaganovich, R. F. Hubbard, A. Ting, T. G. Jones, and P. Sprangle, "Ablative and Discharge Capillaries for Optical Guiding and Velocity Control," in *Advanced Accelerator Concepts, 10th Workshop,* AIP Conference Proceedings 647 (American Institute of Physics, Melville, NY, 2002), p. 165.

k. J. H. Cooley, R. F. Hubbard, D. F. Gordon, A. Zigler, A. Ting, and P. Sprangle., "Effective Electron Beam Injection with Broad Energy Initial Beam," Advanced Accelerator Concepts Workshop, June, 2004; also to appear in workshop proceedings.

l. D. F. Gordon, B. Hafizi, R. F. Hubbard, D. Kaganovich, A. Ting, A. Zigler, J. Cooley, AND P. Sprangle, "Detailed Modeling of Channel Guided Laser Wakefield Accelerators Based on Capillary Discharges," to appear in *Proceedings of the 31st European Physical Society Conference on Plasma Physics*, June-July, 2004 (invited talk).

m. D. F. Gordon, A. Ting, T. Jones, B. Hafizi, R. F. Hubbard, and P. Sprangle, "Particle-in-Cell Simulations of Optical Injectors for Plasma Accelerators," in *Proceedings of the 2003 Particle Accelerator Conference*, p. 1846.

n. D. Kaganovich, A. Ting, D. Gordon, T. G. Jones, E. Briscoe, R. Hubbard and P. Sprangle, "Optical Injection in a Laser Wake Field Accelerator," 2003 APS-DPP Meeting, Albuquerque, NM, Oct. 27-31, 2003 (Poster).